AN ABSTRACT OF THE THESIS OF

Kelley Ruehl for the degree of Master of Science in Mechanical Engineering
presented on May 19, 2011.

Title:

Time-Domain Modeling of Heaving Point Absorber Wave Energy Converters, Including Power Take-Off and Mooring

Abstract approved: _____

Dr. Robert Paasch

Wave energy conversion is still in its infancy, and in order for it to become a commercially viable technology, developers, investors and utilities need to estimate a Wave Energy Converter's (WEC's) performance for the wave climate of a potential installation site. With the goal of estimating a design's power output when subject to stochastic ocean waves, a time-domain modeling methodology was developed for point absorber WECs with arbitrary device geometry. This methodology uses the geometry's unique frequency-domain hydrodynamic response to determine the point absorber's time-domain impulse response functions. By implementing the point absorber's impulse response functions, time-domain equations of motion are defined and the WEC's heave displacement and velocity are solved for in a WEC Dynamics Model developed in MATLAB/Simulink. The modeling methodology is first validated for a single-body point absorber with complex geometry by comparison with experimental data. Then the methodology is applied to a two-body point

absorber geometry that is representative of designs currently being pursued. The time-domain point absorber model is extended to include a hydraulic power take-off system model that estimates the wave energy converter's power output when subject to real ocean waves. Finally, results are presented from the combined WEC dynamics and hydraulic power take-off system model when subject to time-series wave surface elevation from NDBC Umpqua Offshore buoy 46229.

Time-Domain Modeling of Heaving Point Absorber Wave Energy Converters, Including Power Take-Off and Mooring

by

Kelley Ruehl

A THESIS

submitted to

Oregon State University

in partial fulfillment of
the requirements for the
degree of

Master of Science

Presented May 19, 2011
Commencement June 2011

Master of Science thesis of Kelley Ruehl presented on May 19, 2011.

APPROVED:

Major Professor, representing Mechanical Engineering

Head of the School of Mechanical, Industrial, and Manufacturing Engineering

---

Dean of the Graduate School

I understand that my thesis will become part of the permanent collection of Oregon State University libraries. My signature below authorizes release of my thesis to any reader upon request.

Kelley Ruehl, Author

ACKNOWLEDGEMENTS

First of all, I would like to thank my parents for their unwavering support. They have always given me freedom to make my own decisions, and encouraged me to do whatever I want with my life even when it meant moving thousands of miles away. I cannot thank them enough because without them and their support, I would not be the person I am today.

I also want to thank my sister Julie who manages to always bring a smile to my face, no matter what else is going on in life. Whether its a late night phone call to tell me about something hilarious that happened back home, or belting out a song together in Lola, my sister always shows me how to see the light.

Outside of my family, I would like to thank my friends from home, and the new friends I have met in Corvallis. Specifically I would like to thank my boyfriend Mike who has somehow managed to stand by my side during these trying times, and Sahar who has allowed me to still be girly while surrounded by a group of male engineers. Additionally, I want to thank the best Craigslist roommates ever, Sarah and Rachel.

This thesis would not have been possible without the support of my fellow mechanical engineering wave energy graduate students, Steve Meicke, Justin Hovland, Pukha Lenee-Bluhm, and Blake Boren. They helped my research by providing insight through thought provoking conversation, and paper reviews as well as mental relief over beer. This thesis would also not be possible without Bret Bosma who contributed significantly through his knowledge of signal processing and other electrical engineering aspects of wave energy conversion.

Finally, I would like to thank my advisors Dr. Robert Paasch and Dr. Ted Brekken for their guidance, patience, and support through my graduate studies. I would also like to thank Dr. Solomon Yim for providing me with a fundamental understanding of offshore structural dynamics. Additionally, I would like to thank the US Department of Energy for funding my research through the creation of the Northwest National Marine Renewable Energy Center.

CONTRIBUTION OF AUTHORS

Dr. Robert Paasch and Dr. Ted Brekken contributed to the ideas behind both papers, and Justin Hovland, Steve Meicke, and Blake Boren provided suggestions for their revisions. Dr. Solomon Yim contributed to the fundamental understanding of structural dynamics in ocean waves, and Bret Bosma assisted in the implementation of both models in MATLAB/Simulink.

TABLE OF CONTENTS

Page

1 Introduction 1

1.1 Introduction to Wave Energy Conversion 1

1.2 Wave Energy Converter Modeling 1

2 Point Absorber Wave Energy Converter Model 4

2.1 Abstract 5

2.2 Introduction 5

2.3 Wave Energy Converter Modeling 7

2.4 Point Absorber Modeling Methodology 9

2.5 Single-Body Point Absorber Model 11

2.5.1 Equations of Motion 12

2.5.2 Frequency Domain Response 14

2.5.3 Time-Domain Impulse Response Functions 17

2.5.4 WEC Dynamics Model 19

2.6 Two-Body Point Absorber Model 25

2.6.1 Equations of Motion 26

2.6.2 Frequency Domain Response 28

2.6.3 Time-Domain Impulse Response Functions 29

2.6.4 WEC Dynamics Model 31

2.7 Conclusions 36

2.8 Acknowledgments 37

3 Hydraulic Power Take-Off System Model 38

3.1 Abstract 39

3.2 Introduction 39

3.3 Point Absorber 41

3.3.1 Point Absorber Equations of Motion 41

3.3.2 Point Absorber Model Structure 46

3.4 Hydraulic Power Take-Off 49

3.4.1 PTO System Dynamics 49

3.4.2 PTO System Model 53

3.4.3 PTO System Results 55

3.5 Conclusions 57

3.6 Acknowledgments 58

4 Combined Point Absorber and Hydraulic Power Take-Off System Model 59

TABLE OF CONTENTS (Continued)

Page

5 Conclusions 62

Bibliography 62

Appendices 67

A Mooring Force Determination 68

B L10 Hydraulic PTO Model 71

LIST OF FIGURES

Figure Page

2.1 Wave Energy Converter Technologies: (from top left) Wavegen Limpet, Wave Dragon, OPT PowerBuoy, and Pelamis [8, 7, 5, 6] 7

2.2 Flowchart of Point Absorber WEC Modeling Methodology 10

2.3 Single-Body Point Absorber: (left) Single-Body Point Absorber Geometry, (right) Generic Single-Body Point Absorber Model 11

2.4 Single-Body Point Absorber Frequency-Domain Excitation: (top) Excitation Magnitude, (bottom) Excitation Phase 16

2.5 Single-Body Point Absorber Frequency-Domain Radiation: (top) Radiation Damping, (bottom) Added Mass 17

2.6 Single-Body Point Absorber Time-Domain Excitation IRF 18

2.7 Single-Body Point Absorber Time-Domain Radiation IRF 19

2.8 Simulink Single-Body Point Absorber Model: Top Level 21

2.9 Simulink Single-Body Point Absorber Model: WEC Dynamics Subsystem 21

2.10 Viscous Damping Tuned to Match Experimental RAOs, and Average of 9-13 [s] Wave Periods 22

2.11 Single-Body Point Absorber Heave RAOs 23

2.12 Single-Body Point Absorber Irregular Wave Response: (top) Wave and WEC Displacement, (bottom) WEC Velocity 25

2.13 Two-Body Point Absorber: (left) L10 Point Absorber, (right) Generic Two-Body Point Absorber Model 26

2.14 L10 Wave Energy Converter Meshed in AQWA 29

2.15 Two-Body Point Absorber Time-Domain Excitation IRFs 30

2.16 Two-Body Point Absorber Time-Domain Radiation IRFs 31

2.17 Simulink Two-Body Point Absorber Model: Top Level 33

2.18 Simulink Single-Body Point Absorber Model: WEC Dynamics Subsystem 33

2.19 Two-Body Point Absorber Irregular Wave Response: (top) Wave and WEC Displacement, (bottom) Relative Velocity 35

3.1 Two body generic point absorber WEC, [5]. 42

LIST OF FIGURES (Continued)

Figure		Page
3.2	Two body point absorber WEC modeling structure.	48
3.3	PA WEC Dynamics Subsystem.	49
3.4	Hydraulic Power Take-Off System	51
3.5	PTO and Control Subsystem for a Hydraulic PTO	54
3.6	High Pressure Accumulator Subsystem	54
3.7	Hydraulic Variable Displacement Motor Subsystem	55
3.8	Sample Hydraulic PTO Model Output	56
4.1	Flowchart of Combined WEC and PTO Modeling Methodology	60
4.2	L10 Irregular Wave Response: (top) Wave and WEC Displacement, (middle) Relative Velocity, (bottom) Volumetric Flow	61
4.3	L10 Hydraulic PTO: (top) Pressure Difference, (bottom) Power	61

LIST OF TABLES

Table Page

2.1 Single-Body Point Absorber Dimensions 15

2.2 Two-Body Point Absorber Dimensions 28

LIST OF APPENDIX FIGURES

Figure Page

A.1 Experimental Mooring Configuration: Side View, courtesy of RE Vision 68

A.2 Experimental Mooring Configuration: Side View, courtesy of RE Vision 69

A.3 Mooring System Heave Displacement 69

B.1 Hydraulic Piston 71

Chapter 1 – Introduction

1.1 Introduction to Wave Energy Conversion

Earth has a limited supply of the natural resources primarily used to fuel the growing population's ever increasing energy needs. This, in combination with the desire to curtail global climate change motivates research into new and innovative ways to harness energy. Wave energy is a promising frontier because it offers an energy source that is both clean and renewable. Wave Energy Converters (WECs) are devices designed to convert the constant motion of ocean waves into usable power. For review of the basic concepts behind wave energy conversion and description of the breadth of existing WEC technologies, refer to McCormick's book Ocean Wave Energy Conversion [34].

While wave energy conversion has been conceptualized for over a century, the technology is primarily in the stage of research and development. Wave energy developers, or "pioneers", that are furthest along have proved functionality of their design by testing in wave tanks or in the open ocean. However, the only full-scale WEC deployed and producing electricity is the Wavegen Limpet, a shore-based oscillating water column that is deployed on the Scottish island of Islay.

1.2 Wave Energy Converter Modeling

In order for wave energy to become a commercially viable technology, researchers, developers, investors and utilities need to know how WECs will perform when

subject to stochastic ocean waves. The research presented in this thesis is an effort to determine point absorber WECs dynamic response to incoming waves, and what the device's power output will be. Since WECs are subject to ocean waves, for the work presented in this thesis, an understanding of Linear Wave Theory and vibrational analysis is assumed. Refer to Dean and Dalrymple's book Water Wave Mechanics for Engineers and Scientists for a review of Linear Wave Theory [16]. Additionally, for an in depth description of how to model wave energy systems using the concepts of Linear Wave Theory and vibrational analysis, refer to Falnes' book Ocean Waves and Oscillating Systems [24].

This thesis contains two WEC modeling manuscripts, each of which describe an independent model intended for use in the initial design stage to estimate device performance. The first manuscript presents a point absorber WEC modeling methodology, and introduces the WEC Dynamics Model developed in MATLAB/Simulink. The WEC Dynamics Model solves for the point absorber's dynamics when subject to ocean waves, and can be used as an initial design tool to estimate a design's performance for a given wave climate. The WEC modeling methodology is first applied to model a single-body point absorber with a geometry representative of current designs being pursued. The single-body point absorber model is then validated by comparison with experimental wave tank data. Next, the WEC modeling methodology is applied to model OSU's L10, a two-body point absorber design.

In the second manuscript, a hydraulic Power Take-Off (PTO) system is defined and a Hydraulic PTO Model, developed in MATLAB/Simulink, is described. The Hydraulic PTO Model solves for the power output of the hydraulic system when subject to the WEC's relative velocity. While the Hydraulic PTO Model was developed as a subsystem to the WEC Dynamics Model, for the power output

results presented in this manuscript, the WEC's relative velocity is prescribed, it is not determined from the WEC Dynamics Model.

Finally, results from the combined WEC Dynamics and Hydraulic PTO Model are presented when used to model OSU's L10 two-body point absorber with a hydraulic PTO system. Output from the combined WEC Dynamics and Hydraulic PTO Model include the WEC's dynamic response to real ocean waves, and the corresponding power out of the hydraulic system due to the WEC's relative motion. The combined dynamics model is used to demonstrate the modularity of the modeling structure developed in MATLAB/Simulink, and how the design tool can be used to estimate overall device performance.

Chapter 2 – Point Absorber Wave Energy Converter Model

Time-Domain Modeling of Heaving Point Absorber Wave Energy Converters

Kelley Ruehl, Robert Paasch, Ted K.A. Brekken, and Bret Bosma

Oregon State University

Corvallis, Oregon 97330

Email: ruehlkm@gmail.com

Submitted to Journal of Offshore Mechanics and Arctic Engineering

2.1 Abstract

In order to promote and support development of the wave energy industry, a time-domain Wave Energy Converter (WEC) modeling methodology was developed for use in the initial design stage. The modeling methodology can be applied to heaving point absorber WECs with arbitrary device geometry to estimate their performance for a given wave climate. First, the WECs frequency-domain response is solved for, and then it is used to develop time-domain equations of motion which are implemented and solved for in MATLAB/Simulink. The modeling methodology is first applied to a single-body point absorber with complex geometry and validated against experimental data. Then the methodology is used to model a two-body point absorber consisting of a heaving buoy and spar/plate.

2.2 Introduction

Wave Energy Converters (WECs) are devices designed to convert the constant motion of ocean waves into usable power. Despite being conceptualized and patented for over a century, WECs still remain largely in the phase of research and development [34]. According to a technology assessment performed by the US Department of the Navy in 2009, most wave energy developers are in the initial stages of device development corresponding to Technology Readiness Levels (TRLs) 2-6 [11]. Wave energy developers with highest TRLs 6-10 have proved the functionality of their design by performing scale model tests of their design in controllable wave tank environments or in the open ocean [6, 5, 2, 4]. The only developer that has achieved TRL 9, corresponding to full-scale deployment and production of electricity, is the Wavegen Limpet which has been deployed on the Scottish island of

Islay since 2000 [8].

In order to promote development of the wave energy industry, current wave energy research is largely influenced by developer needs and lessons learned from related industries. Because of this, wave energy research topics are broad, ranging from environmental and resource assessments to WEC farm interactions and material testing [17, 14, 31, 30]. Ultimately for a wave energy project to be successful, in addition to public support, researchers, developers, investors and utilities need to estimate the device's performance before deployment. In the wind industry, generic turbine models were developed to estimate a turbine's performance for a particular wind resource. The goal of this research is to develop similar publicly available models for WECs that can be used to estimate a device's performance for a potential site's wave climate.

Unlike the wind industry where the three-bladed horizontal axis wind turbine has become the predominant design, there are many different WEC technologies being actively pursued. These WEC technologies are shown in Figure 2.1 and include: Oscillating Water Columns (OWCs), overtopping devices and oscillating bodies. OWCs are devices that utilize the cyclic compression and decompression of air above the wave surface to run a turbine. The shore-based Limpet OWC developed by WaveGen is shown in Figure 2.1. Overtopping devices, like the Wave Dragon shown in Figure 2.1, focus waves toward an elevated basin which is used to run water through a low head turbine. Oscillating bodies are devices that operate by floating on the water surface and converting the body's motion into usable power. As shown in Figure 2.1, oscillating bodies are typically split into two subcategories: attenuators and point absorbers. Attenuators are large in extension and consist of multiple bodies connected by hinges that articulate along the direction of wave propagation. The Pelamis shown in Figure 2.1 is an

example of an attenuator. Point absorbers, represented by the OPT Powerbuoy in Figure 2.1, are much smaller than the incoming wavelength and operate by oscillating in heave with the wave. The oscillating body's motion is then converted into usable power typically through either a hydraulic or direct drive power take-off system. Due to the diversity of existing WEC technologies, one model will not be capable of accurately representing all WECs, so it is necessary to develop models for each technology. This research focuses on developing a methodology that can be used to model heaving point absorber WECs with arbitrary device geometry.

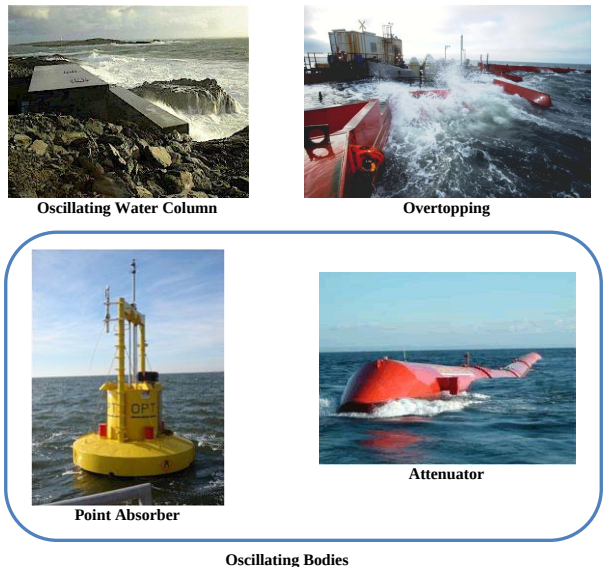

Figure 2.1: Wave Energy Converter Technologies: (from top left) Wavegen Limpet, Wave Dragon, OPT PowerBuoy, and Pelamis [8, 7, 5, 6]

2.3 Wave Energy Converter Modeling

Point absorber WECs are oscillating bodies subject to stochastic ocean waves which are composed of many waves with different frequencies and directions. Because of this, a natural progression is to model point absorbers in the frequency-

domain using the principle of linear superposition. However, while frequency-domain modeling is a valuable tool for linear system analysis, WECs are subject to many non-linearities such as those from power take-off systems, control strategies, end stops, and complex mooring systems. Time-domain models of heaving point absorber WECs with idealized geometries have been developed by wave energy researchers in order to accurately capture these non-linearities and evaluate device performance.

For example, Falcao modeled a point absorber as a heaving hemisphere with a hydraulic power take-off system and implemented different methods of control [21, 22]. Kara modeled a heaving hemisphere point absorber in order to compare a point absorber's power absorption with and without latching control [29]. A heaving cylinder point absorber was modeling by Ricci in order to compare its performance with a hydraulic versus a direct drive power take-off system [35]. Eidsmoen modeled a heaving cylinder point absorber with a hydraulic power take-off system and end stops to estimate yearly power output with and without phase control [19]. These are all examples of point absorbers modeled in the time-domain as a single-body with a basic geometry, however point absorber designs currently pursued by developers are rarely single-body WECs with basic geometries.

The OPT PowerBuoy and Wavebob are both examples of two-body point absorbers WECs with complex geometries that convert the relative motion between two heaving bodies into usable power [5, 9]. In order to represent these more complicated WEC designs, Candido and Eidsmoen have independently extended time-domain modeling of single-body point absorbers to develop two-body point absorber models [13, 18]. However, a model that can be used to estimate the performance of a point absorber that accounts for arbitrary device geometry has not been established. The goal of this research is to develop a publicly available

time-domain model and methodology that can be applied to any heaving point absorber WEC to estimate performance.

2.4 Point Absorber Modeling Methodology

The point absorber WEC modeling methodology presented in this paper is intended for use as an initial design tool to estimate the performance of a point absorber WEC with arbitrary geometry for a specified wave climate. It is a time-domain model restricted to heave motion only since heave is the degree of freedom in which most point absorbers extract power. In reality, the point absorber will move in all six degrees of freedom (corresponding to heave, sway, surge, yaw, pitch and roll), but for the purpose of simplification the model solves for heave motion only.

A flowchart presenting the point absorber WEC modeling methodology is shown in Figure 2.2. The first step is to define the 3D WEC geometry. Once the 3D geometry is created, it is then imported into a frequency-domain hydrodynamic analysis code where the WEC's frequency-domain hydrodynamic response is solved. For the results presented in this paper ANSYS AQWA was used [10]. Next, the complex frequency-domain excitation force, $f_e(i\omega)$, is used to calculate the time-domain excitation Impulse Response Function (IRF), $f_e(t)$, the frequency-domain radiation $f_r(\omega)$ is used to calculate the time-domain radiation IRF, $f_r(t)$, and the limit at infinity of the frequency-domain added mass is evaluated, $A(\infty)$. These hydrodynamic terms, $f_e(t)$, $f_r(t)$ and $A(\infty)$, are the building blocks of the time-domain WEC Equations of Motion (EOM) that will be defined in a later section. Once the hydrodynamic terms are determined, the user can define regular or irregular waves as input to the WEC Dynamics Model developed in MAT-

LAB/Simulink [33]. The WEC Dynamics Model solves the governing time-domain EOM for the WEC's displacement and velocity and calls on a Mooring System Model that uses that WEC's displacement and velocity to determine the mooring force imparted on the WEC. By using the WEC's frequency-domain hydrodynamic response to develop time-domain EOM, the WEC modeling methodology presented in Figure 2.2 accounts for arbitrary device geometry, and can thus be used to compare many different WEC designs.

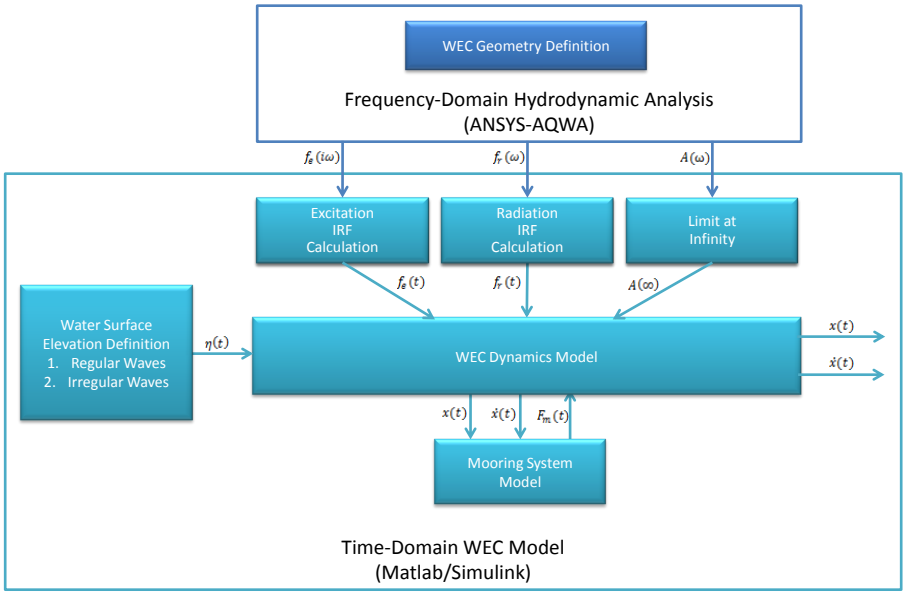

Figure 2.2: Flowchart of Point Absorber WEC Modeling Methodology

In the following sections each step of the point absorber WEC modeling methodology will be described and applied to a specific point absorber design. In Section 4 a single-body point absorber with complex geometry will be modeled using the WEC modeling methodology. Then, in Section 5 the WEC modeling methodology will be applied to model a two-body point absorber.

2.5 Single-Body Point Absorber Model

The single-body point absorber is modeled as one rigid body consisting of a buoy, spar, and damping plate, as shown on the left side of Figure 2.3. This geometry was chosen because it is representative of point absorbers designs currently being developed, with the simplification of being modeled as one rigid body. Additionally, this single-body WEC geometry has experimental data available from wave tank testing, and results from a RANS simulation [32, 42]. The experimental data for the single-body geometry was used to validate the WEC Dynamics model presented in this paper, results which will be presented in Section 4.4. The right side of Figure 2.3 demonstrates how a generic single-body point absorber model can be applied to a specific WEC design. The generic single-body model consists of a WEC of mass m, heaving in the x direction. The point absorber model is subject to an incident wave $\eta(t)$, and is moored to the sea floor at water depth h.

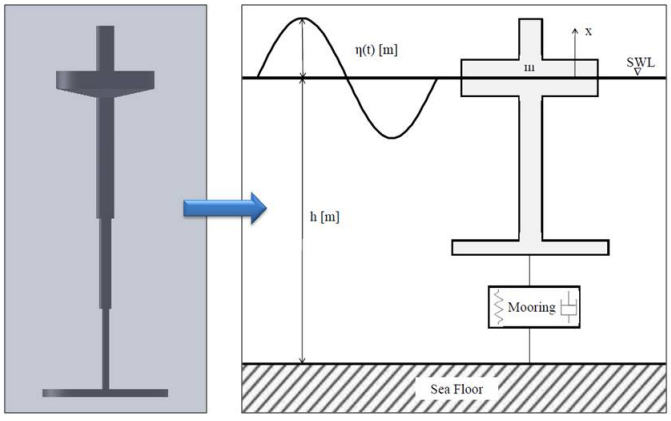

Figure 2.3: Single-Body Point Absorber: (left) Single-Body Point Absorber Geometry, (right) Generic Single-Body Point Absorber Model

2.5.1 Equations of Motion

Before applying the point absorber modeling methodology, it is important to first understand the model's governing equations. The single-body point absorber time-domain EOM are formulated based on the integro-differential EOM for ship motions in six degrees of freedom. These time-domain EOM use the IRF formulation and were first introduced by Cummins for ship motions in 1962 [15]. This formulation uses the ship's IRFs to account for the fluid-structure interaction of the ship with the wave. Due to obvious similarities between ship motions and WEC dynamics, the Cummins formulation can be modified to represent a single-body heaving point absorber as shown in Eq. (3.1), where x represents the WEC's heave motion.

$$F_e(t) - F_r(t) - F_m(x, \dot{x}) = K_{hs}x + b_v\dot{x} + (m + A(\infty))\ddot{x} \tag{2.1}$$

The left hand side of Eq. (3.1) consists of forcing functions that account for the WEC's interaction with incident waves and the mooring system. The first term is the excitation force, or the force the incoming wave imparts on the WEC. The excitation force, $F_e(t)$, is calculated via Eq. (3.2) by the convolution of the water surface elevation, $\eta(t)$, with the non-causal excitation IRF, $f_e(t)$. The second term is the radiation force, which is the force the WEC creates by moving and thus radiating waves. The radiation force, $F_r(t)$, is determined by the convolution of the radiation IRF, $f_r(t)$, with the WEC's velocity, $\dot{x}$, as shown in Eq. (3.3). The last term, $F_m(x, \dot{x})$ accounts for the force imparted on the WEC from the mooring system. The mooring force is generally a function of the WEC's displacement and velocity and dependent on the mooring stiffness, k_m, and damping, b_m, as defined

on the top line of Eq. (3.4).

$$F_e(t) = \int_{-\infty}^{\infty} \eta(\tau) f_e(t-\tau) d\tau \tag{2.2}$$

$$F_r(t) = \int_{-\infty}^{t} f_r(t-\tau) \dot{x}(\tau) d\tau \tag{2.3}$$

$$\begin{aligned} F_m(x, \dot{x}) \quad &= k_m x + b_m \dot{x} \\ &= 8k_m \left(1 - \frac{l_m}{\sqrt{{l_m}^2 + x^2}}\right) x \end{aligned} \tag{2.4}$$

Since the single-body point absorber geometry was chosen in order to be validated against experimental data, the mooring force was determined based on the experimental setup used by Li [32]. The experimental setup had eight mooring lines in total, each with stiffness k_m of 160 $[kN/m]$ and initial length l_m equal to 1.7 $[m]$. The mooring configuration consisted of two layers of crosses that were fixed to the walls of the wave tank, initially in a horizontal position. The equivalent mooring force felt by the WEC in the heave direction, determined using trigonometric relationships, is a function of the WEC's displacement only as defined on the second line of Eq. (3.4).

The terms on the right hand side of point absorber EOM defined in Eq. (3.1) are similar to a mass-spring-damper system with terms multiplied by the WEC's displacement, velocity and acceleration. These terms are the hydrostatic stiffness, K_{hs}, viscous damping, b_v, and the added mass at infinite wave frequency, $A(\infty)$. The hydrostatic stiffness is multiplied by the WEC's displacement to determine the restoring force of the water on the body known as the the hydrostatic force, $F_{hs}(t)$, defined in Eq. (2.5). The hydrostatic stiffness is equal to the product of

the density of sea water, ρ_{sw} equal to $1,025$ $[kg/m^3]$, acceleration due to gravity, g equal to 9.81 $[m/s^2]$, and the cross sectional area of the point absorber, A, at the still water level. In the single-body point absorber model the hydrostatic stiffness is a constant, K_{hs} equal to $955,580$ $[N/m]$, which means A is also a constant. Viscous damping, b_v, is a correctional term used to account for viscous effects that are not otherwise accounted for in the time-domain EOM. The process used to determine the viscous damping constant will be described in Section 4.4. The added mass, $A(\omega)$, is a frequency dependent term that represents the additional force required to move a mass in water compared to the force required to move the same mass in air. The single-body point absorber EOM calls for the limit of the added mass as the wave frequency approaches infinity, $A(\infty)$.

$$F_{hs}(t) = K_{hs}x = \rho_{sw}gAx \tag{2.5}$$

2.5.2 Frequency Domain Response

In order to implement the single-body point absorber EOM defined in the previous section, the WEC's hydrodynamics response must be determined. The frequency-domain hydrodynamic response is then used to determine the WEC's excitation IRF, radiation IRF, and added mass at infinity which are the building blocks of the time-domain point absorber EOM. The 3D geometry of the single-body point absorber shown on the left of Figure 2.3, with dimensions defined in Table 2.1, was imported into ANSYS AQWA where the WEC's frequency-domain response was determined. AQWA is a boundary element method code based on the principles of linear wave theory, so the frequency-domain response has the assumptions of incompressible, irrotational, and inviscid flow. The single-body point absorber

was modeled in AQWA with a mass of $250,000$ $[kg]$ at a water depth of 70 $[m]$. While AQWA was used to determine the frequency-domain response presented in this paper, any hydrodynamic code capable of determining frequency-domain excitation, radiation and added mass could be used for the modeling methodology.

Table 2.1: Single-Body Point Absorber Dimensions

Buoy	Diameter	11 [m]
	Height	2 [m]
Spar	Diameter	2 [m]
	Height	41.34 [m]
Plate	Diameter	14 [m]
	Height	0.84 [m]

The single-body point absorber's complex frequency-domain hydrodynamic excitation force, $f_e(i\omega)$, is shown in Figure 2.4 and the WEC's radiation force, $f_r(\omega)$, and added mass, $A(\omega)$, are shown in Figure 2.5. In order to properly calculate heave IRFs, the frequency-domain response should have a truncation frequency of 2 $[rad/s]$ with a frequency spacing of 0.01 $[rad/s]$ [38]. When the WEC geometry is imported into a frequency-domain hydrodynamic code, the mesh should be sized to meet these requirements because the mesh determines the frequency range response the code solves for. The results presented in Figure 2.4 and Figure 2.5 use linear interpolation and extrapolation to determine response with the appropriate spacing at low-frequencies. Based on the single-body point absorber's frequency-domain added mass, the infinite added mass, $A(\infty)$, was determined to be $1,225,100$ $[kg]$.

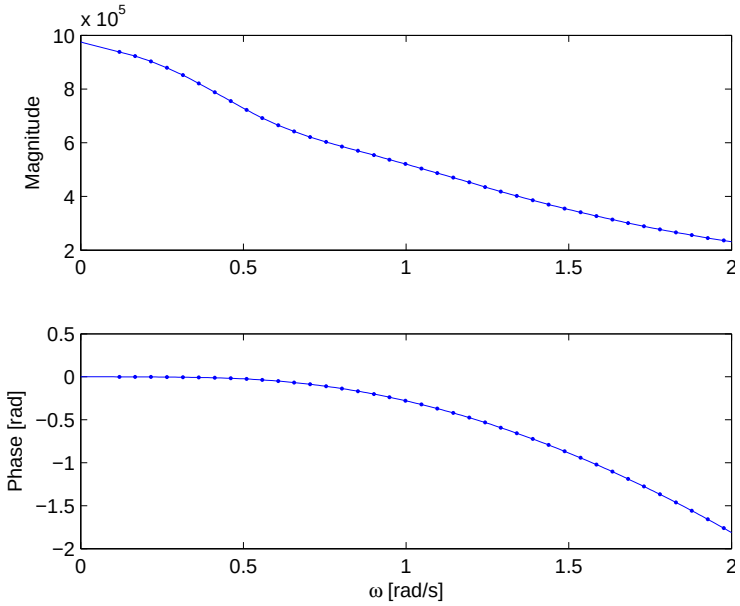

Figure 2.4: Single-Body Point Absorber Frequency-Domain Excitation: (top) Excitation Magnitude, (bottom) Excitation Phase

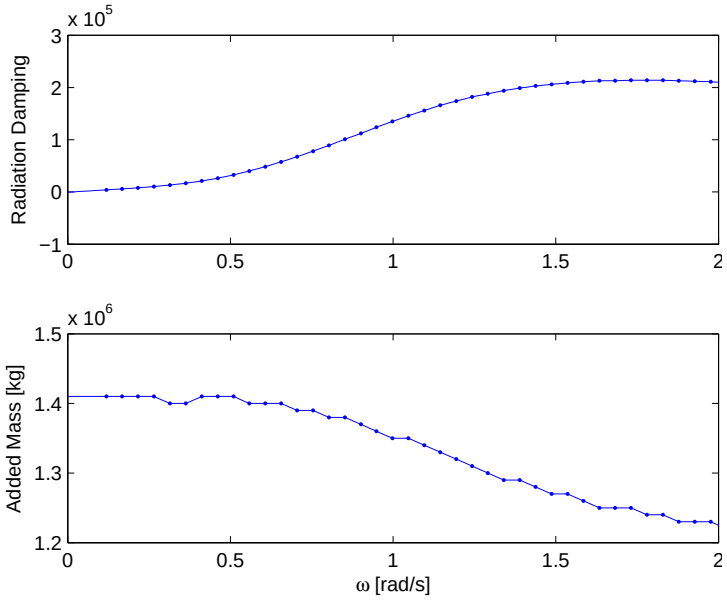

Figure 2.5: Single-Body Point Absorber Frequency-Domain Radiation: (top) Radiation Damping, (bottom) Added Mass

2.5.3 Time-Domain Impulse Response Functions

After the single-body point absorber's frequency-domain response is determined, the hydrodynamic terms are used to calculate the WEC's time-domain IRFs. For the single-body point absorber EOM, an excitation IRF and a radiation IRF must be calculated. The non-causal time-domain excitation IRF is calculated via Eq. (2.6) using the frequency-domain excitation magnitude and phase [23]. The causal time-domain radiation IRF is calculated by Eq. (3.7) using the WEC's frequency-domain radiation. The single-body point absorber's calculated non-causal time-domain excitation IRF is shown in Figure 2.6, and the causal time-domain radiation IRF is shown in Figure 2.7. These IRFs were calculated using

trapezoidal integration in MATLAB.

$$f_e(t) = \frac{1}{2\pi} \int_{-\infty}^{\infty} f_e(i\omega) e^{i\omega t} d\omega \tag{2.6}$$

$$f_r(t) = \frac{2}{\pi} \int_{0}^{\infty} f_r(\omega) cos(\omega t) d\omega \tag{2.7}$$

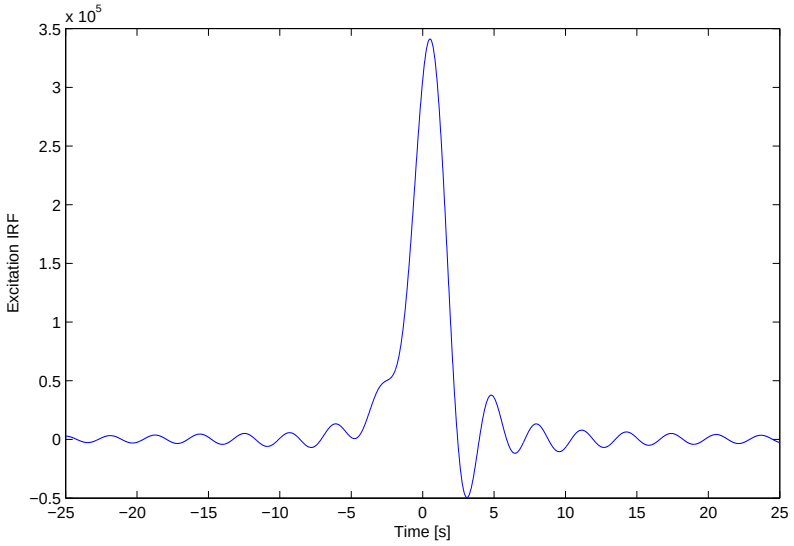

Figure 2.6: Single-Body Point Absorber Time-Domain Excitation IRF

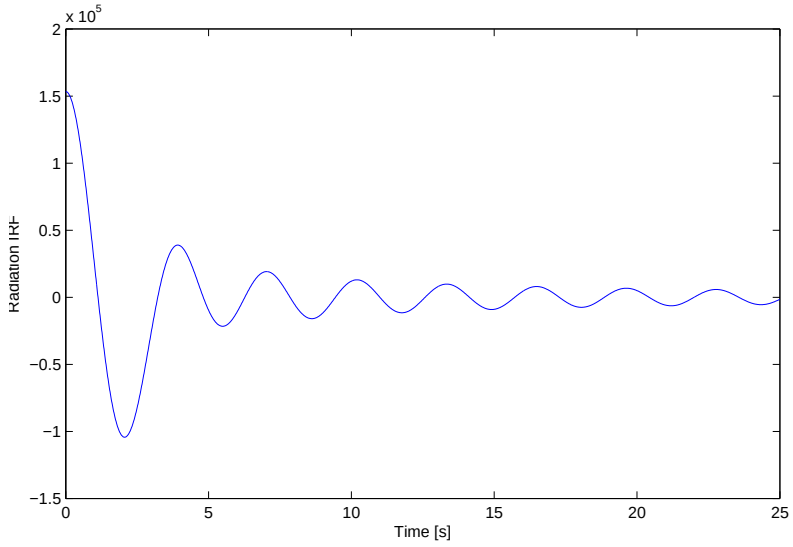

Figure 2.7: Single-Body Point Absorber Time-Domain Radiation IRF

2.5.4 WEC Dynamics Model

Once the single-body point absorber's IRFs are calculated, time-series wave surface elevation must be defined, then the governing EOM can be solved for the WEC's displacement and velocity in the MATLAB/Simulink WEC Dynamics Model. Using the WEC modeling methodology presented in Figure 2.2, regular and irregular wave time-series can be used to run the WEC Dynamics Model. For the results shown in this paper, the time-series wave surface elevation is imported directly from NDBC Umpqua Offshore buoy 46229 which is deployed off the coast of Oregon north of Reedsport [3]. The time-series is from June 2008, which represents a relatively low energy wave climate according to seasonal trends [31]. In the following sections, first the MATLAB/Simulink WEC Dynamics Model will be introduced by describing the model's systems and subsystems, then output from the

WEC Dynamics Model will presented in addition to results from the single-body point absorber model validation.

2.5.4.1 WEC Dynamics Model Structure

The single-body point absorber WEC Dynamics model takes the wave surface elevation, $\eta(t)$, as its input and solves for the WEC's displacement and velocity. The top level of the WEC Dynamics Model implemented in Simulink, shown in Figure 2.8, defines the model's input and its outputs as well as its subsystems: Excitation Force Determination, WEC Dynamics, and Mooring Force Determination. The Excitation Force Determination subsystem calculates the excitation force due to the incident wave on the WEC, $F_e(t)$, according to Eq. (3.2). The WEC Dynamics subsystem, shown in Figure 2.9, implements Eq. (3.1) by taking the excitation and mooring forces as its inputs and solving for the WEC's displacement and velocity. In this subsystem, a Finite Impulse Response (FIR) filter is used to determine the radiation force, $F_r(t)$, by convolving the WEC's radiation IRF with the WEC's velocity according to Eq. (3.3). The last subsystem on the top level of the WEC Dynamics Model is the Mooring Force Determination. In this subsystem, the force the mooring system imparts on the single-body point absorber is calculated using the second line of Eq. (3.4).

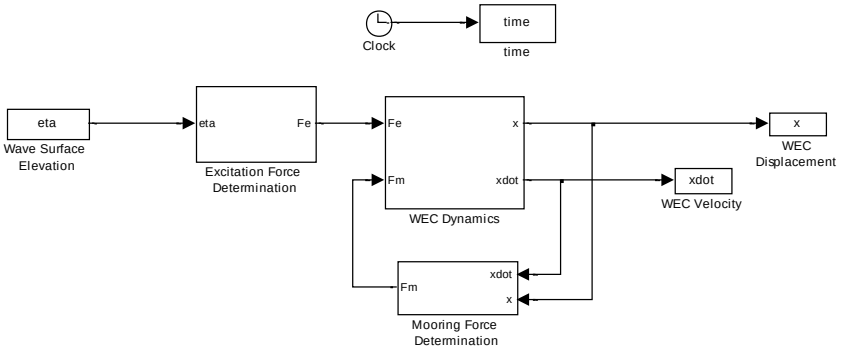

Figure 2.8: Simulink Single-Body Point Absorber Model: Top Level

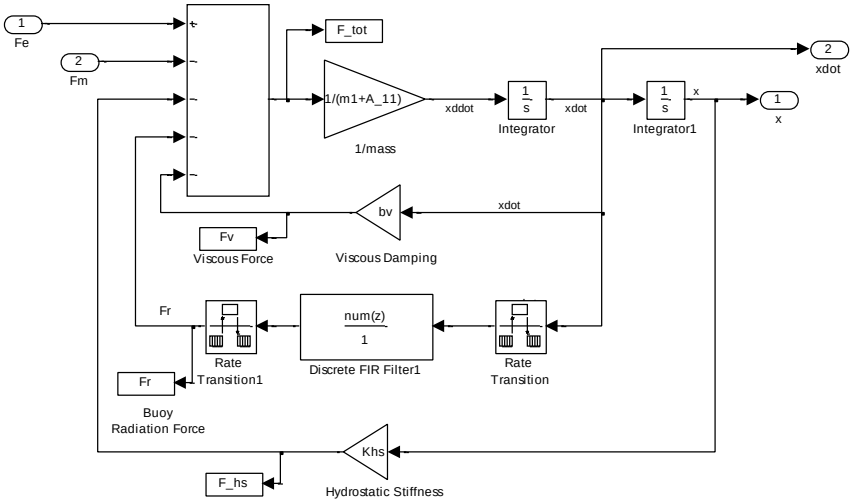

Figure 2.9: Simulink Single-Body Point Absorber Model: WEC Dynamics Subsystem

2.5.4.2 WEC Dynamics Model Output

The geometry for the single-body point absorber model was chosen because experimental data from wave tank testing is available to validate the WEC modeling methodology for this geometry. The experimental data was used to determine the viscous damping term defined in Eq. (3.1) for the single-body point absorber geometry through the following process. First, the single-body WEC Dynamics Model was run with regular wave input to determine the heave Response Amplitude Operators (RAOs) for a 3 $[m]$ wave height. The RAO is defined as the magnitude of the heave response divided be the amplitude of the incoming wave. A tuned b_v value was determined for each wave period by matching the RAOs from the WEC Dynamics Model with the experimental heave RAOs, these tuned b_v values are shown in Figure 2.10.

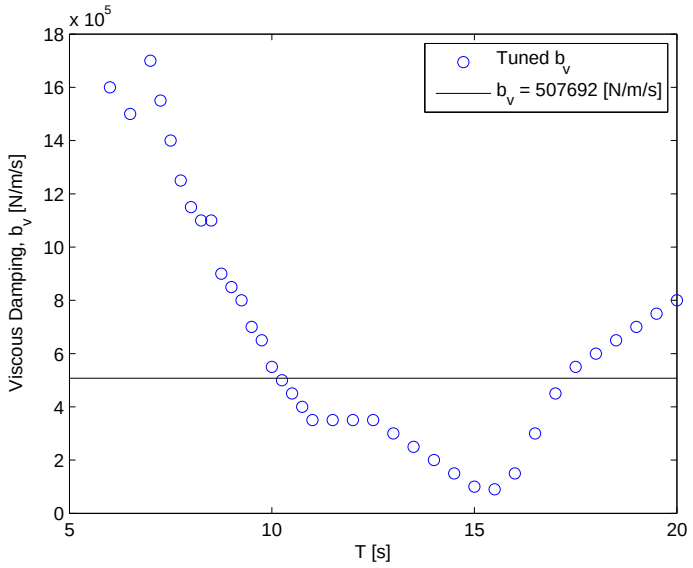

Figure 2.10: Viscous Damping Tuned to Match Experimental RAOs, and Average of 9-13 [s] Wave Periods

In order to determine the single-body point absorber's response to irregular waves, a constant viscous damping term, $b_v = 507,692\ [N/m/s]$, was chosen by averaging the tuned b_v values for 9 to 13 $[s]$ wave periods which are representative of the Oregon wave climate. The RAO from the single-body point absorber WEC Dynamics Model using the averaged viscous damping term is compared with the experimental heave RAOs in Figure 2.11. While the resultant RAOs do not match the experimental RAOs well for low periods, these results show that the WEC Dynamics Model provides an accurate estimate of the single-body point absorber's response for Oregon's dominant wave periods. Alternatively, the viscous damping term could be chosen to match lower wave periods to estimate response for a different wave climate.

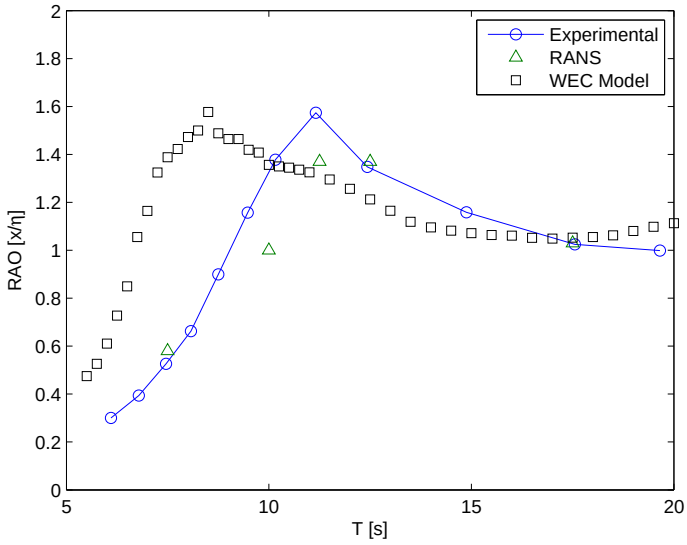

Figure 2.11: Single-Body Point Absorber Heave RAOs

For further comparison, Figure 2.11 also includes RAOs from a RANS simulation for the same single-body point absorber geometry [32]. The RANS simulation estimates experimental RAOs well for the wave periods tested, however this is a much more computationally demanding simulation. The RANS simulation took upwards of 8 hours to solve on 64 cores, whereas the WEC Dynamics Model solves in less than 30 seconds. These modeling approaches perform different types of analysis, and are intended for different stages in development. A RANS simulation is best suited for modeling a final WEC design in cases where there is highly non-linear interaction between the wave and the WEC, such as a wave breaking on the WEC. Whereas the WEC modeling methodology presented in this paper is intended for use as an initial design tool to estimate a WEC's performance.

Once the viscous damping term for single-body point absorber model is determined, the WEC Dynamics Model can be used to estimate the WEC's response to irregular waves. The top of Figure 2.12 shows the wave-surface elevation from NDBC buoy 46229 in June 2008 with the WEC's displacement response, and the bottom shows the WEC's corresponding velocity which is an important term because it drives the Power Take-Off (PTO) system. The response in Figure 2.12 shows a phase shift between the incoming wave and the single-body point absorber's displacement response, with the WEC's velocity ranging within +/- 1 $[m/s]$. In Section 4 the WEC modeling methodology has been used to model a single-body point absorber, and validated against experimental data. Similar to Section 4, in Section 5 the WEC modeling methodology will be applied to a two-body point absorber geometry.

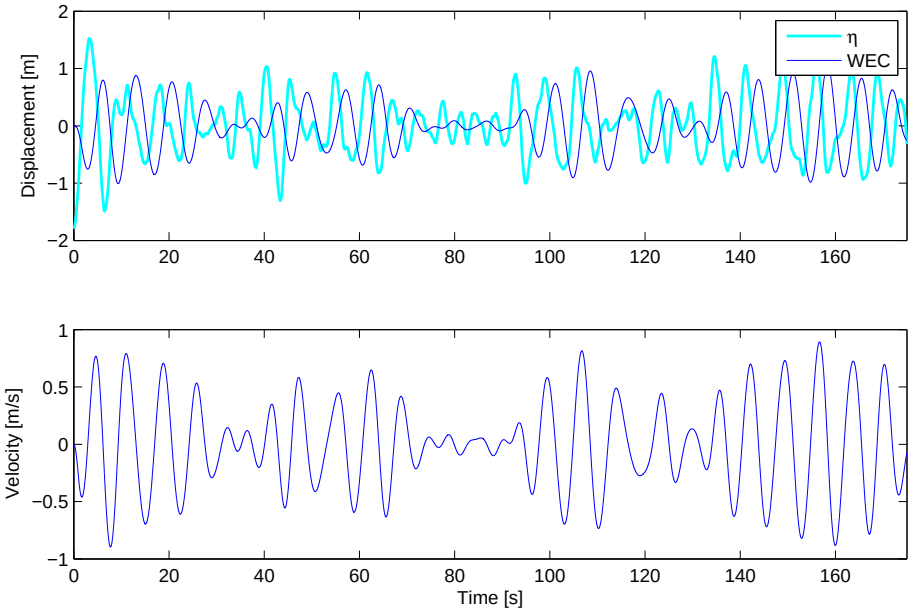

Figure 2.12: Single-Body Point Absorber Irregular Wave Response: (top) Wave and WEC Displacement, (bottom) WEC Velocity

2.6 Two-Body Point Absorber Model

Previously, the point absorber modeling methodology was applied and validated for a single-body geometry. In the following sections the modeling methodology is used to model a two-body point absorber and the WEC Dynamics Model developed in MATLAB/Simulink is extended to account for the additional complexity of interacting bodies. To demonstrate how the modeling methodology can be applied to a two-body point absorber, Figure 2.13 shows how the L10 point absorber on the left can be represented by a generic two-body point absorber model on the right. The L10 is a two-body point absorber designed by Oregon State University in collaboration with Columbia Power Technologies that was tested off the coast of Newport, Oregon in 2008 [20]. The generic two-body point absorber model

consists of a buoy of mass m_1, heaving in the x_1 direction, and a spar/plate of mass m_2, heaving in the x_2 direction. While the L10 is modeled without a drag plate, the second body is referred to as the spar/plate because many two-body designs incorporate a drag plate. Similar to the single-body point absorber, the two-body point absorber is subject to an incident wave $\eta(t)$, and the spar/plate is moored to the sea floor at water depth h.

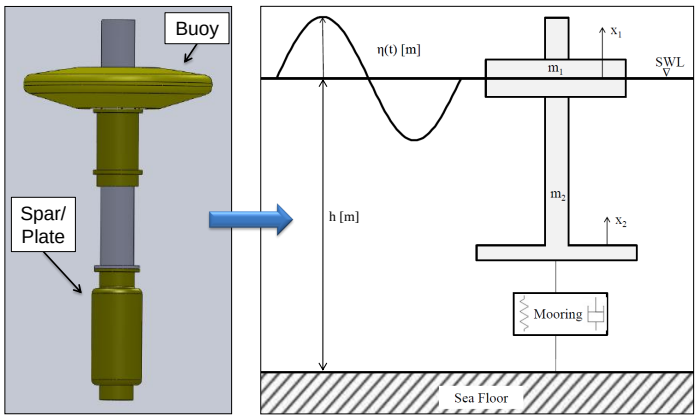

Figure 2.13: Two-Body Point Absorber: (left) L10 Point Absorber, (right) Generic Two-Body Point Absorber Model

2.6.1 Equations of Motion

The two-body point absorber EOM are similar to the single-body point absorber EOM defined in Eq. (3.1). The buoy and spar/plate EOM each have a viscous damping term, and the excitation and radiation forces calculated in the same way. However the two-body point absorber EOM have additional forcing terms that were not accounted for in Eq. (3.1). The two-body point absorber has governing EOM defined by Eq. (3.8) for the buoy, and Eq. (3.9) for the spar/plate. These EOM are derived from the two-body point absorber EOM used by Eidsmoen [18].

With a two-body WEC design, there are a coupling radiation interaction forces due to each body's motion, $F_{r_{12}}(t)$ and $F_{r_{21}}(t)$. The buoy's motion radiates waves which influence the spar/plate's motion, defined by Eq. (3.10), and the spar/plate's motion also radiates waves that in turn influence the buoy's motion, defined by Eq. (3.11). In the two-body point absorber model the hydrostatic stiffness is assumed to be a constant, K_{hs} equal to $96,743$ $[N/m]$, a value determined based on the cross-sectional area of the buoy at the still water level. Since the mooring system is connected to the spar/plate, Eq. (3.9) has a mooring force term due to the force the mooring system imparts on it. The mooring force, $F_m(x_2, \dot{x}_2)$, is typically a function of the spar/plate's displacement and velocity. The same mooring system defined for the single-body model was used for the two-body model, and is defined in the second line of Eq. (3.4). Now that fundamental understanding of the WEC model's governing EOM has been established, the first step in the modeling methodology is to create a WEC geometry and determine its frequency domain response, this process will be described in the next section.

$$\begin{aligned} F_{e_1}(t) &- F_{r_{11}}(t) - F_{r_{12}}(t) \\ &= K_{hs}x_1 + b_{v_1}\dot{x}_1 + (m_1 + A_{11}(\infty))\ddot{x}_1 \end{aligned} \tag{2.8}$$

$$\begin{aligned} F_{e_2}(t) &- F_{r_{22}}(t) - F_{r_{21}}(t) - F_m(x_2, \dot{x}_2) \\ &= b_{v_2}\dot{x}_2 + (m_2 + A_{22}(\infty))\ddot{x}_2 \end{aligned} \tag{2.9}$$

$$F_{r_{12}}(t) = \int_{-\infty}^{t} f_{r_{12}}(t-\tau)\dot{x}_2(t)d\tau + A_{12}(\infty)\ddot{x}_2 \tag{2.10}$$

$$F_{r_{21}}(t) = \int_{-\infty}^{t} f_{r_{21}}(t-\tau)\dot{x}_1(t)d\tau + A_{21}(\infty)\ddot{x}_1 \tag{2.11}$$

2.6.2 Frequency Domain Response

Once a WEC's 3D geometry is modeled, the next step is to determine the WEC's frequency-domain response using a hydrodynamic code. This step is necessary because the frequency-domain response is used to calculate time-domain IRFs, which are needed to define the two-body point absorber EOM, (3.8) and (3.9). The 3D geometry of L10 WEC was modeled using the dimensions defined in Table 2.2, then it was imported into ANSYS AQWA and meshed, as shown in Figure 2.14. The two-body point absorber was modeled with $m_1 = 2,625.3$ $[kg]$ and $m_2 = 2,650.4$ $[kg]$ at a water depth of 100 $[m]$. AQWA is then used to solve for the frequency-domain hydrodynamic complex excitation force, $f_e(i\omega)$, radiation force coefficient, $f_r(\omega)$, and added mass, $A(\omega)$, for both the buoy and spar/plate, all terms which are necessary to solve the two-body point absorber EOM. The two-body point absorber's frequency-domain added mass is used to determine the buoy's infinite added mass, $A_{11}(\infty) = 8866.7$ $[kg]$, the spar/plate's infinite added mass, $A_{22}(\infty) = 362$ $[kg]$, and the coupled added mass, $A_{12}(\infty) = A_{21}(\infty) = 362$ $[kg]$.

Table 2.2: Two-Body Point Absorber Dimensions

Buoy	Diameter Height	3.5 [m] 0.76 [m]
Spar/Plate	Diameter Height	1.1 [m] 7.03 [m]

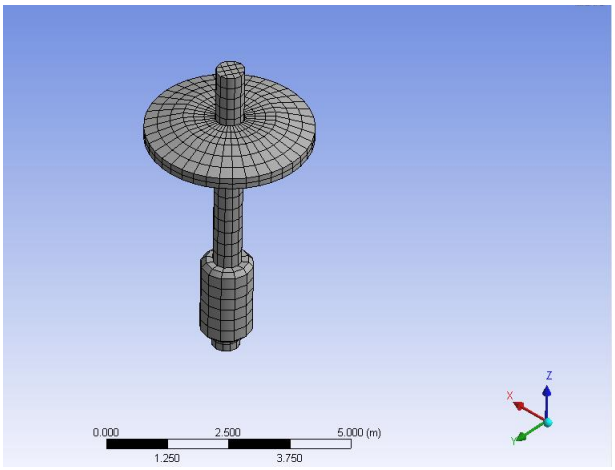

Figure 2.14: L10 Wave Energy Converter Meshed in AQWA

2.6.3 Time-Domain Impulse Response Functions

After the L10's frequency-domain response is determined using a hydrodynamic code, the complex excitation force, $f_e(i\omega)$, and radiation force coefficient, $f_r(\omega)$ are used to calculate the WEC's time-domain IRFs. For the two-body point absorber EOM, excitation IRFs must be calculated for the buoy, and spar/plate and radiation IRFs must be calculated for the buoy, spar/plate and coupled interaction. The non-causal time-domain excitation IRFs are calculated via Eq. (2.6) using the frequency-domain excitation magnitude and phase, and the causal time-domain radiation IRFs are calculated via Eq. (3.7) using the frequency-domain radiation coefficient. The L10's calculated non-causal buoy and spar time-domain excitation IRFs are shown in Figure 2.15, and the causal buoy, spar/plate, and coupled time-domain radiation IRFs are shown in Figure 2.16.

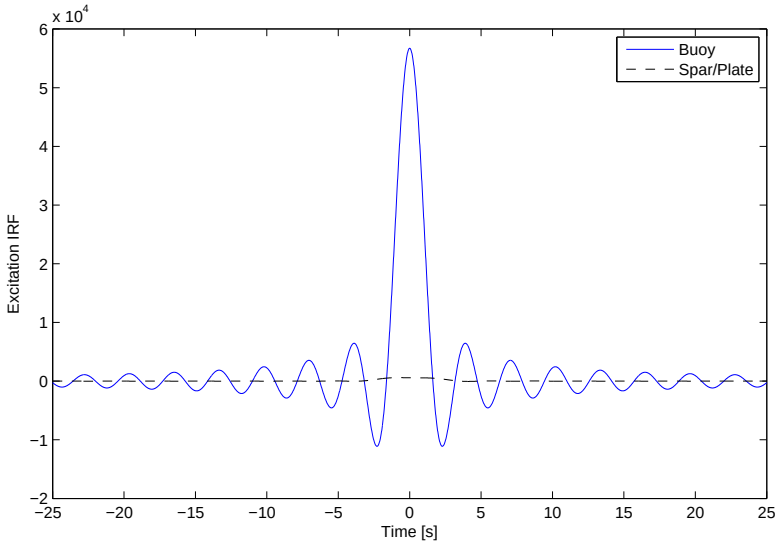

Figure 2.15: Two-Body Point Absorber Time-Domain Excitation IRFs

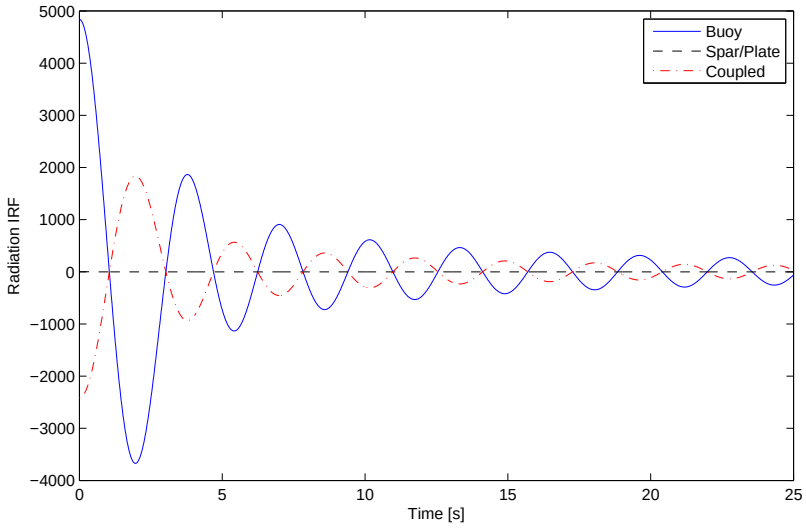

Figure 2.16: Two-Body Point Absorber Time-Domain Radiation IRFs

2.6.4 WEC Dynamics Model

Once the two-body point absorber's time-domain IRFs are calculated, the next step is to solve the governing EOM for the WEC's displacement and velocity. The two-body point absorber EOM defined in Eq. (3.8) and Eq. (3.9) are implemented and solved in MATLAB/Simulink. First, the MATLAB/Simulink two-body WEC Dynamics Model will be introduced by describing the function of the model's systems and subsystems. Then output from the two-body WEC Dynamics Model will be presented for the same irregular wave surface elevation used for the single-body point absorber. The time-series wave surface elevation used is from NDBC buoy 46229 data in June 2008.

2.6.4.1 WEC Dynamics Model Structure

Similar to the single-body WEC Dynamics Model, the two-body WEC Dynamics Model takes the wave surface elevation, $\eta(t)$, as its input and solves for the velocity and displacement of the buoy and spar/plate. The top level of the two-body WEC Dynamics Model as implemented in Simulink is shown in Figure 2.17. The top level of the model defines the system's input and its outputs as well as its subsystems: Excitation Force Determination, WEC Dynamics, and Mooring Force Determination. The Excitation Force Determination subsystem calculates the excitation force due to the incident wave on the buoy, $F_{e_1}(t)$, and on the spar/plate, $F_{e_2}(t)$. The Mooring Force Determination subsystem calculates the force the mooring system imparts on the WEC as a function of the spar/plate's displacement and velocity, $F_m(x_2, \dot{x}_2)$, using the second line of Eq. (3.4). The WEC Dynamics subsystem, shown in Figure 2.18, shows the modeling structure that solves for the two-body WEC dynamics consisting of the following subsystems: Buoy Dynamics, Coupling Radiation Damping Force, and Spar/Plate Dynamics. The Buoy Dynamics subsystem implements Eq. (2.5) and solves for the buoy's displacement and velocity, and the Spar/Plate Dynamics subsystem implements Eq. (2.6) and solves for the spar/plate's displacement and velocity. Both the Buoy Dynamics and the Spar/Plate Dynamics subsystems are very similar in structure to the single-body point absorber subsystem shown in Figure 2.9. The Coupling Radiation Damping Force subsystem uses Eq. (3.7) and Eq. (3.8) to determine the coupling radiation force between the buoy and then the spar/plate.

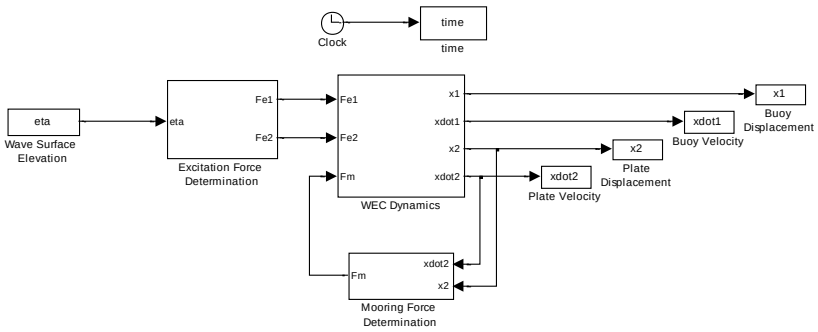

Figure 2.17: Simulink Two-Body Point Absorber Model: Top Level

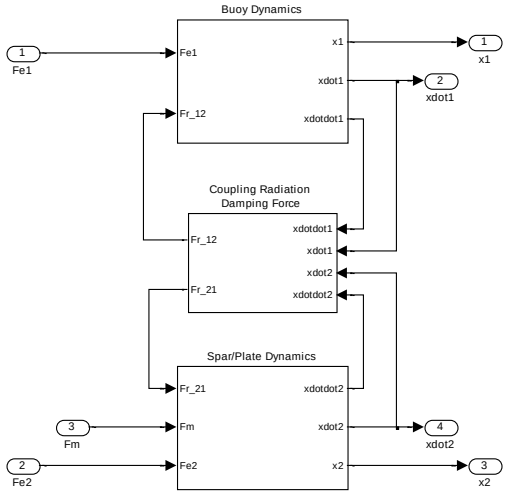

Figure 2.18: Simulink Single-Body Point Absorber Model: WEC Dynamics Subsystem

2.6.4.2 WEC Dynamics Model Output

The two-body WEC Dynamics Model developed in MATLAB/Simulink is then used to estimate the L10's response when subject to real ocean waves collected by NDBC buoy 46229. Before running the model, the viscous damping terms defined in Eq. (3.8) and Eq. (3.9), b_{v_1} and b_{v_2}, must be determined. These terms are constants included in the two-body point absorber EOM to account for viscous effects that are otherwise ignored in this modeling methodology. Ideally, appropriate viscous damping terms would be determined by matching experimental RAOs with the model's RAOs, however unlike the single-body point absorber geometry, there is no experimental wave tank data available for the L10 (or any other two-body point absorber).

Since the WEC modeling methodology presented in this paper is intended for use as an initial design tool, it is not uncommon that a geometry will be modeled prior to experimental wave tank testing. Because of this, it is recommended that initial viscous damping terms are chosen based on the following criteria. The viscous damping term should be chosen so that the model converges to a stable solution near resonance and eliminates high-frequency vibration; otherwise, the model is an underdamped system with RAOs spiking near resonance. For the L10, these criteria were met with viscous damping terms $b_{v_1} = 5,000\ [N/m/s]$ and $b_{v_2} = 50,000\ [N/m/s]$. Furthermore, it is recommended that once experimental data is collected, the viscous damping terms should be refined using the process described in the single-body point absorber section.

Once the viscous damping terms for two-body point absorber model are determined, the WEC Dynamics Model can be used to estimate the WEC's response to irregular waves. The wave surface elevation is plotted with the buoy

and spar/plate's heave displacement response on the top of Figure 2.19, and the velocity of the buoy relative to the spar/plate, $\dot{x}_2 - \dot{x}_1$, is plotted on the bottom. For the relatively low energy wave climate of June, the WEC's relative velocity typically ranges from +/- 2 $[m/s]$, a term that is especially important term because it drives the PTO system.

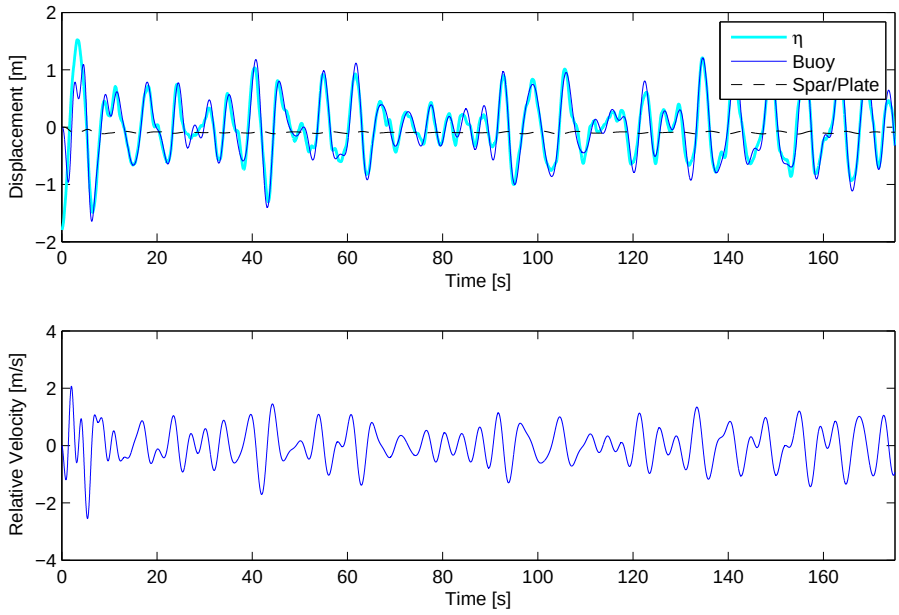

Figure 2.19: Two-Body Point Absorber Irregular Wave Response: (top) Wave and WEC Displacement, (bottom) Relative Velocity

2.7 Conclusions

As an effort to promote and support development of the wave energy industry, a modeling methodology was developed than can be used to estimate the performance of point absorber WECs for a given wave climate. This modeling methodology is presented as a flowchart in Figure 2.2, and is applicable for modeling both single-body and two-body point absorbers with arbitrary geometry. The first step is to determine the frequency-domain response of a point absorber's 3D geometry. Impulse response functions are then calculated from the point absorber's frequency-domain response, and they are used to define the governing time-domain equations of motion. Time-series wave surface elevation is then used as the input to the WEC Dynamics Model developed in MATLAB/Simulink that solves for the point absorber's response.

The modeling methodology was first applied to a single-body point absorber geometry representative of designs currently being pursued. Then experimental wave tank data for the same geometry was used to determine a viscous damping term appropriate for the Oregon wave climate. This value was determined by averaging the tuned viscous damping terms for Oregon's dominant wave periods, 9 to 13 $[s]$. Using this viscous damping term, the response amplitude operators from the single-body WEC Dynamics Model were compared to experimental response and results from a RANS simulation for the same single-body point absorber geometry, shown in Figure 2.11. For the dominant wave periods of interest, the response determined from the single-body WEC Dynamics Model is very good, typically with less than 10% error by comparison with experimental data.

The modeling methodology was then applied to model Oregon State University's L10 two-body point absorber. Unlike the single-body geometry, there is

currently no experimental wave tank data publicly available for two-body point absorbers even though they are a common design. Viscous damping terms for the two-body model were determined by two criteria: eliminate high frequency vibration and converge to a stable solution near resonance. Since the modeling methodology is intended for use as a fast solving design tool, it is not uncommon that experimental data will not be available for a particular geometry. However, it is recommended that once experimental data is available, it should be used to refine the model similar to what was done for the single-body geometry.

A benefit of modeling in MATLAB/Simulink is its modular nature which allows the WEC Dynamics Model to be extended to include a power PTO subsystem on the top level that can be used to estimate the device's power output. Currently a hydraulic PTO system model is under development to be incorporated into the WEC Dynamics Model [36]. The modularity of this model makes it well suited for comparing WEC performance with different PTO systems by simply using a different subsystem. Additionally, since MATLAB/Simulink is often used to develop control strategies, another possible extension of the WEC Dynamics model is to implement and evaluate different methods of control.

2.8 Acknowledgments

This work was supported by Sandia National Laboratories and the Northwest National Marine Renewable Energy Center (NNMREC) under Department of Energy Award Number DE-FG36-08GO18179.

Chapter 3 – Hydraulic Power Take-Off System Model

Large-Scale Ocean Wave Energy Plant Modeling

Kelley Ruehl, Ted K.A. Brekken, Bret Bosma, and Robert Paasch

Oregon State University

Corvallis, Oregon 97330

Email: ruehlkm@gmail.com

Proceedings of the 2010 IEEE Conference on Innovative Technologies for an Efficient and Reliable Electricity Supply

IEEE/CITRES 2010

27-29 Sept. 2010, Waltham, MA

CITRES.2010.5619775

3.1 Abstract

In order for wave energy conversion to be a commercially viable technology, wave energy researchers, developers, investors and utilities need an estimate of a wave energy converter's (WEC) power output at a potential installation site. The wind industry has developed generic turbine models that capture the general dynamics of large-scale proprietary wind turbine designs in order to estimate a turbine's power output for a given wind climate. Similar generic models need to be developed for WECs. Current WEC deigns vary significantly in design and technology. The focus of this paper is on developing a generic model structure for one of the prominent WEC designs, the two body point absorber. The model structure is developed by using time domain equations of motion (EOM) to define systems and subsystems as well as their corresponding inputs and outputs. The generic model structure is then extended by developing a hydraulic power take-off (PTO) system model.

3.2 Introduction

Converting the constant motion of ocean waves into a usable energy source by means of a Wave Energy Converter (WEC) has been conceptualized by inventors and engineers for over a century, however its implementation is largely still in the research and development stage [34]. The WEC developers that are furthest along in the Research and Development process have full scale WECs deployed in the ocean; some of these companies include Pelamis, Ocean Power Technologies (OPT), Aquamarine Power and WaveGen [6, 5, 1, 8]. The vast majority of WEC developers are designing and testing scale models of their devices, including Columbia Power Technologies (CPT) and SEAREV [2, 28].

Since the wave energy industry is still in Research and Development, there is much that can be learned from the experiences of developers in related industries in order to make wave energy a commercially viable technology. In the wind industry, for example, several generic turbine models have been created to capture the general wind turbine dynamics of large-scale proprietary wind turbine designs, as well as the dynamics of large-scale wind farms. These models are used to estimate any turbine's power output for a given wind resource. Similar generic models for ocean wave energy converters could be used to estimate power output at a potential installation site and would be beneficial to wave energy researchers, developers, investors and utilities alike.

While there are many parallels between the industry developments of the wind energy and the wave energy industry, there are also significant differences. Unlike in the wind industry where the three-bladed, horizontal axis wind turbine has become the predominant design, WECs vary greatly in both design and technology. WECs are typically classified into the following categories: oscillating water columns, overtopping devices, and oscillating bodies. Oscillating water columns are typically shore-based and operate by running a turbine that extracts energy through cyclic compression and decompression of a volume of air trapped above the wave surf ace. Overtopping devices focus waves toward an elevated basin which is used to run water through a low head turbine. Oscillating bodies are devices that operate by floating on the water surface and converting the motion of the body to usable power. They are often further classified into subcategories of either attenuators or point absorbers. Attenuators are devices large in extension, consisting of multiple bodies connected by hinges that articulate along the direction of wave propagation. Point absorbers are much smaller than the incoming wavelength and operate by oscillating in heave with the wave. The oscillating body's motion is then converted

into usable power typically through either a hydraulic or direct drive power take-off (PTO) system. Each of the aforementioned WEC categories will require its own generic model.

This paper presents a methodology for modeling a generic two body point absorber WEC that estimates power output for a given wave climate. The first section of the paper introduces a generic point absorber design and defines its equations of motion. Then an overall model structure for a generic point absorber WEC is proposed by defining systems and subsystems as well as their corresponding inputs and outputs. The remainder of the paper provides extension of the generic model structure by developing a hydraulic PTO system model.

3.3 Point Absorber

3.3.1 Point Absorber Equations of Motion

The purpose of this generic model is to capture the general dynamics of a point absorber WEC in order to estimate power output of the device. The first step to accurately model a device is to formulate an understanding of how the device works, and determine which characteristics are important to capture. Point absorbers are often modeled as a single heaving body, whose motion relative to the ground is used to run a PTO [29]. While this approach gives an approximation of the power output of a point absorber, it is a simplification of the real device. Point absorbers are designed to be deployed in water depths between 40-60m. At these depths it is uncommon for the buoy to be connected to a PTO system that is directly connected to the ground. Instead, most point absorber designs consist of two bodies, a heaving buoy and a damping plate. The buoy is connected through

a PTO system to the damping plate, which is then moored to the sea floor. A diagram of a generic point absorber consisting of a buoy and damping plate is shown in Figure 3.1. The buoy is excited by an incoming wave and its motion relative to the damping plate is used to run a PTO system that converts this motion to usable power. Point absorbers only produce power output through motion in heave (up and down motion) but are free to move in other degrees of freedom. This model restricts motion of the buoy and plate to heave since it is the relevant degree of freedom.

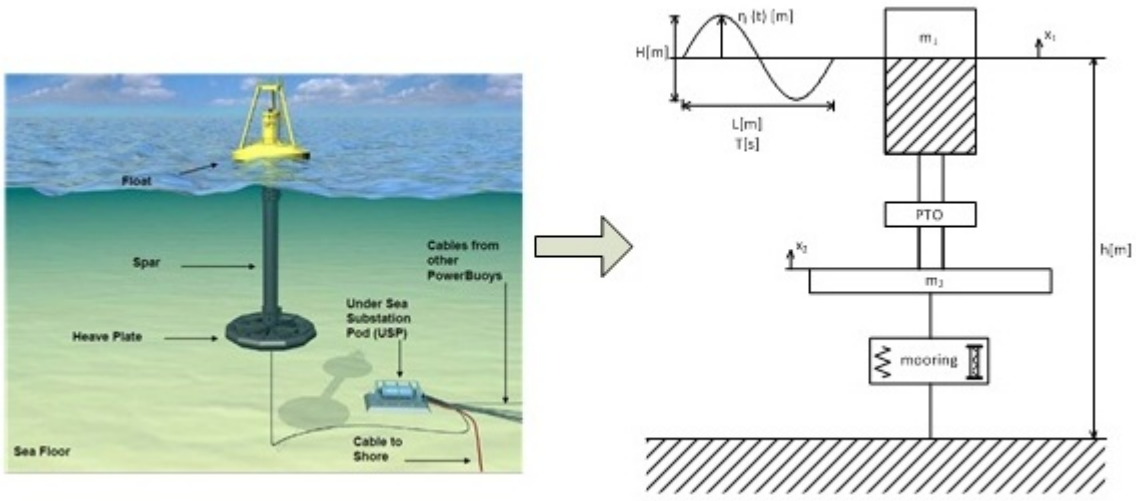

Figure 3.1: Two body generic point absorber WEC, [5].

The time domain equation of motion for a body moving in heave on the water surface has a formulation similar to a mass-spring-damper system, with the addition of a few forcing terms that account for the fluid-structure interaction of the WEC with the water. Implementation of the impulse response function to create an integro-differential Equation of Motion (EOM), as shown in Eq. (3.1), was first introduced by Cummins for ship motions [15].

$$\int_{-\infty}^{\infty} \eta(t) f_e(t-\tau) d\tau - \int_{-\infty}^{t} \dot{x}(t) k_r(t-\tau) d\tau = (k + \rho_{sw} g A)x + (m + A(\infty))\ddot{x} \quad (3.1)$$

This formulation is based on Linear Wave Theory (LWT) and assumes incompressible, irrotational flow with small amplitude motion. The first term in the equation is the excitation force, $F_e(t)$, which is the force the incoming wave imparts on the body. The excitation force is determined by the convolution of the water surface elevation, $\eta(t)$, with the non-causal excitation impulse response function, $f_e(t)$, as shown in Eq. (3.2).

$$F_e(t) = \int_{-\infty}^{\infty} \eta(t) f_e(t-\tau) d\tau \quad (3.2)$$

The second term in the heaving body's EOM is the radiation force, which is the force the body creates by moving and thus radiating waves. The radiation force, $F_r(t)$, is determined by the convolution of the radiation impulse response function, $k_r(t)$, with the body's velocity, $\dot{x}(t)$, as shown in Eq. (3.3).

$$F_r(t) = \int_{-\infty}^{t} \dot{x}(t) k_r(t-\tau) d\tau \quad (3.3)$$

The terms on the right hand side of Eq. (3.1) are similar to a mass-spring-damper system, where m represents the body's mass, k is the body's inherent stiffness, and b is its damping. The additional terms are the hydrostatic force, F_{hs}, and the added mass, $A(\infty)$. The hydrostatic force is the restoring force of the water on the body and is equal to the product of the density of salt water, $\rho_s w$, acceleration due to gravity, g, and the cross sectional area of the body, A, as

shown below in Eq. (3.4). The added mass is a term that represents the additional force required to move a mass in water compared to the force required to move the same mass in air.

$$F_{hs}(t) = \rho_{sw} g A x \tag{3.4}$$

The Cummins integro-differential EOM is for a single body, and does not account for the interaction of two bodies with one another which is the case with the two body generic point absorber design. The buoy will radiate waves that influence the force felt on the plate, and the plate will radiate waves that influence the force felt by the buoy. This is an additional complexity since there is significant coupling between the motions of each body. The Cummins formulation was originally intended for ships, so it does not include mooring or PTO forces which will have a significant impact of the point absorber's motion. These issues were addressed by Falnes and Jeffreys when developing a time domain WEC EOM and by Eidsmoen when modeling a two body point absorber [18, 27, 23]. The EOM for the two body generic point absorber design shown below in Eq. (3.5) for the buoy and Eq. (3.6) for the plate was adapted from the Eidsmoen formulation.

$$F_{e_1} - F_{r_{11}} - F_{r_{12}} + F_{b_1} - F_{PTO}(\dot{x}_1, \dot{x}_2) - b_1\dot{x}_1 - k_1 x_1 - \rho_{sw} g A_1 x_1 = (m_1 + A_{11}(\infty))\ddot{x}_1 \tag{3.5}$$

$$F_{e_2} - F_{r_{22}} - F_{r_{21}} + F_{b_2} - F_{PTO}(\dot{x}_1, \dot{x}_2) - b_2\dot{x}_2 - k_2 x_2 - F_m(x_2, \dot{x}_2) - F_D(\dot{x}_2) = (m_2 + A_{22}(\infty))\ddot{x}_2 \tag{3.6}$$

The additional terms in the two body generic point absorber EOM, Eq. (2.5) and Eq. (2.6), represent the forces created by the interaction of the two bodies, $F_{r_{12}}$ and $F_{r_{21}}$, the force of the PTO system on each of the bodies, F_{PTO}, the buoyancy forces, F_b, the mooring force, F_m and the drag force, F_D. In the buoy EOM, the coupling radiation force, $F_{r_{12}}$, is the force the plate imparts on the buoy through its motion and is determined by Eq. (3.7). There is a similar term in the plate EOM which represents the coupling radiation force the buoy imparts on the plate. This force, $F_{r_{21}}$, is determined by Eq. (3.8).

$$F_{r_{12}}(t) = \int_{-\infty}^{t} k_{r_{12}}(t-\tau)\dot{x}_2(t)d\tau + A_{12}(\infty)\ddot{x}_2 \tag{3.7}$$

$$F_{r_{21}}(t) = \int_{-\infty}^{t} k_{r_{21}}(t-\tau)\dot{x}_1(t)d\tau + A_{21}(\infty)\ddot{x}_1 \tag{3.8}$$

The PTO force appears in both EOMs, and when there is no excitation forcing from a wave, the PTO force must be equal in magnitude with the buoyancy forces of both the plate and the buoy, this is the steady state force balance. The buoyancy force on the buoy is shown in Eq. (3.9), where V_s is the initial submerged volume of the buoy, and m_1 is its mass. The plate also has a buoyancy force, shown in Eq. (3.10), but since it is always submerged it is determined by the plate's total volume, V_2, and its mass m_2.

$$F_{b_1} = g(\rho_{sw}V_s - m_1) \tag{3.9}$$

$$F_{b_2} = g(\rho_{sw}V_2 - m_2) \tag{3.10}$$

The drag plate provides resistance to motion and has a drag force associated with it that is always in the opposite direction of the plate's velocity. As shown in Eq. (3.11), the drag force is determined by the drag coefficient, C_D, which is based on the plate's geometry, the plate's cross sectional area, A_2, and is a function of the plate's velocity, $\dot{x}_2$.

$$F_D = \frac{C_D}{2} A_2 \rho_{sw} |\dot{x}_2| \dot{x}_2 \tag{3.11}$$

Both the mooring and PTO system are represented by black boxes in Figure 3.1, this is because these forces are highly design specific. Since the mooring lines will be directly connected to the damping plate, $F_m(x_2, \dot{x}_2)$ must be a function of the plate's position and velocity. The PTO system converts the relative motion between the buoy and the damping plate into usable power, so $F_{PTO}(\dot{x}_1, \dot{x}_2)$ must be a function of the plate and buoy's respective velocities.

3.3.2 Point Absorber Model Structure

Once the two body generic point absorber EOM have been defined, it is possible to propose an overall model structure by defining systems and subsystems as well as their corresponding inputs and outputs. MATLAB/Simulink was used to develop the model structure because the software can easily and clearly define systems [33]. Once these systems have been defined, the software can also run simulations. Having clearly defined systems and subsystems gives the model a modular structure, allowing for systems to be easily interchanged. For example the modularity of these systems easily allows a developer to compare how their device performs with a direct drive PTO compared to its performance with a hydraulic PTO. Sim-

ilarly, modular system design also allows for easy comparison of different mooring configurations or device geometry.

Previous work has been done using MATLAB/Simulink to model various WECs. Shek et. al used the software to model a single heaving buoy point absorber with direct drive PTO and reactive force control [40]. Yavuz et. al also modeled a single heaving buoy to compare different PTO tuning strategies [37, 41]. These papers were used as a point of reference for their overall model structure, but were limited in that they only modeled one body with the PTO connected directly to the sea floor, and did not include external mooring forces. Previous MATLAB/Simulink modeling was aimed at comparing device performance with different control strategies. The goal of this paper is to develop a modeling structure than can be used for any point absorber WEC to estimate the device's power output when subject to a given wave climate.

The top level of the system model is shown in Figure 3.2. The input block, eta, is the time series wave surface elevation. This input can be from a site's surface elevation collected directly by a wave staff or a data collection buoy, or the time series can be reproduced from spectral records using the random sea simulation method proposed by Tucker [39]. The wave surface elevation is then run through the Excitation Force Determination subsystem that calculates the wave excitation forces felt by the buoy and the plate respectively using Eq. (3.2). This subsystem requires the excitation impulse response function for both the buoy and the plate. Once the excitation forces are calculated, they are input into the Point Absorber (PA) WEC Dynamics subsystem. This subsystem contains the WEC EOM and requires the forces from the PTO and mooring as inputs. The PA WEC Dynamics subsystem solves the WEC EOM for the buoy and plate's respective displacements and velocities. The plate's displacement and velocity are

then input to the Mooring Force Determination subsystem which calculates the mooring force based on a pre-defined mooring configuration. The relative velocity between the buoy and the plate, $\dot{x} = \dot{x}_1 - \dot{x}_2$, is then an input to the PTO and Control subsystem. The PTO and Control subsystem outputs the force the PTO imparts on the WEC, as well as the device's power output. While there are other forces that act on the WEC, only the excitation, mooring and PTO forces are in the top level of the model structure since they are external forces.

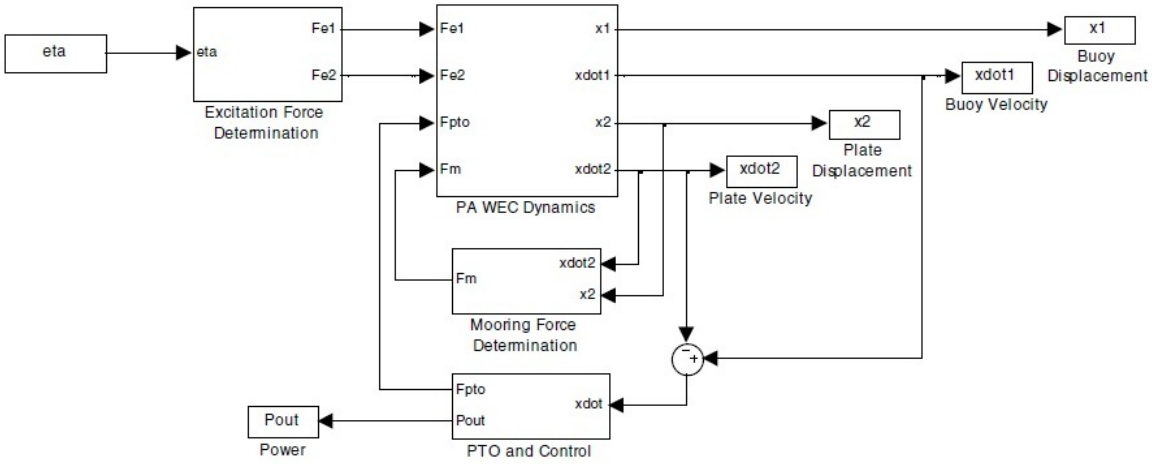

Figure 3.2: Two body point absorber WEC modeling structure.

Within the PA WEC Dynamics subsystem are the Buoy Dynamics, Plate Dynamics, and Coupling Radiation Damping Force subsystems shown in Figure 3.3. The buoy's displacement, velocity and acceleration within the Buoy Dynamics block is shown using Eq. (2.5). This subsystem has the buoy's excitation and buoyancy forces, the PTO force and the coupling radiation force as inputs. In the Plate Dynamics subsystem, Eq. (2.6) is solved for the plate's displacement, velocity and acceleration. The subsystem has the plate's excitation and buoyancy forces, the PTO force, the coupling radiation force, and the mooring force as inputs. The Coupling Radiation Damping Force subsystem calculates the coupling radiation

forces using Eq. (3.7) and Eq. (3.8) and takes the buoy and plate's respective velocities and accelerations as inputs.

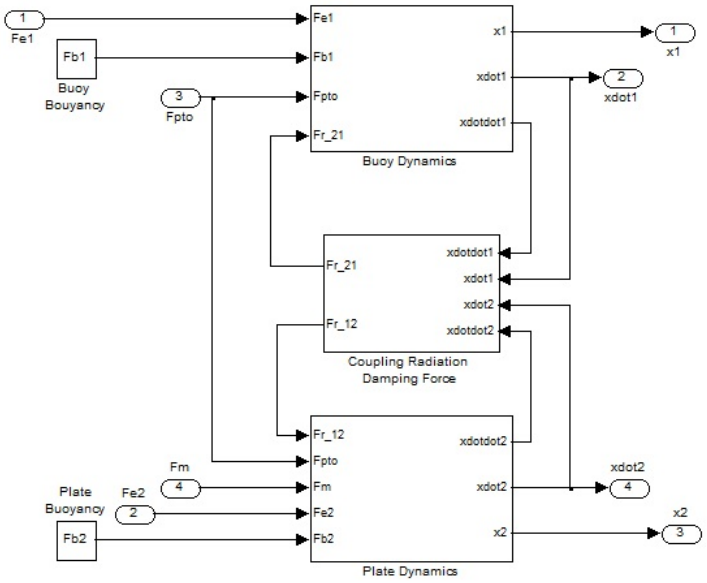

Figure 3.3: PA WEC Dynamics Subsystem.

3.4 Hydraulic Power Take-Off

3.4.1 PTO System Dynamics

Due to the stochastic nature of the ocean environment, power smoothing is a common concern for WEC grid connection. Hydraulic PTO systems are often chosen for WECs over other PTO systems because they have a relatively smoothed power output. Wave energy developers including SEAREV and WaveRoller have implemented hydraulic PTO systems in their scaled model tests of their devices. Full scale devices with hydraulic PTO systems have been developed by Pelamis, Aquamarine Power and OPT [5, 1, 26]. Much research has been done on point

absorbers with hydraulic PTO systems. At the Norwegian Institute of Technology in Trondheim a scale model of the heaving buoy Type E point absorber with a hydraulic PTO system was tested in a wave tank [25]. Falcao developed a hydraulic PTO system model for a heaving buoy point absorber and implemented phase control [21, 22]. Ricci et al. extended the work of Falcao by comparing a similar WEC designs power output with linear PTO system and a hydraulic PTO system [35]. Babarit et al. developed a hydraulic PTO system model for the SEAREV WEC [12]. Previous research has mainly been limited to single body WECs in order to test different control strategies. The goal of this research is to provide an extension of the model structure for a two body generic point absorber by developing a hydraulic PTO system model for this system.

A hydraulic PTO system is a closed loop system that consists of a piston moving inside a cylinder, a control valve, a high pressure (HP) accumulator, a hydraulic motor connected to a generator and a low pressure (LP) accumulator, see Figure 3.4. The hydraulic PTO system converts the relative motion between the bodies into usable power by using the relative motion to push a piston up and down inside a hydraulic cylinder. The motion of the piston creates high and low pressure regions within the cylinder. When the piston is moving down in the cylinder, a high pressure region is created in region B of the cylinder. Once the pressure in region B exceeds the pressure in the HP accumulator, the directional control valve allows hydraulic fluid to be pumped from region B of the cylinder into the HP accumulator. The pressure difference across the HP accumulator and LP accumulator causes hydraulic fluid to run across a hydraulic motor and enter the LP accumulator. The directional control valve then allows the hydraulic fluid to be sucked into region A of the cylinder. A similar process is gone through when the piston is moving upwards, except in this case high pressure is created in region

A of the cylinder and flow goes from region A, into the HP accumulator, across the motor, into the LP accumulator and into region B of the cylinder.

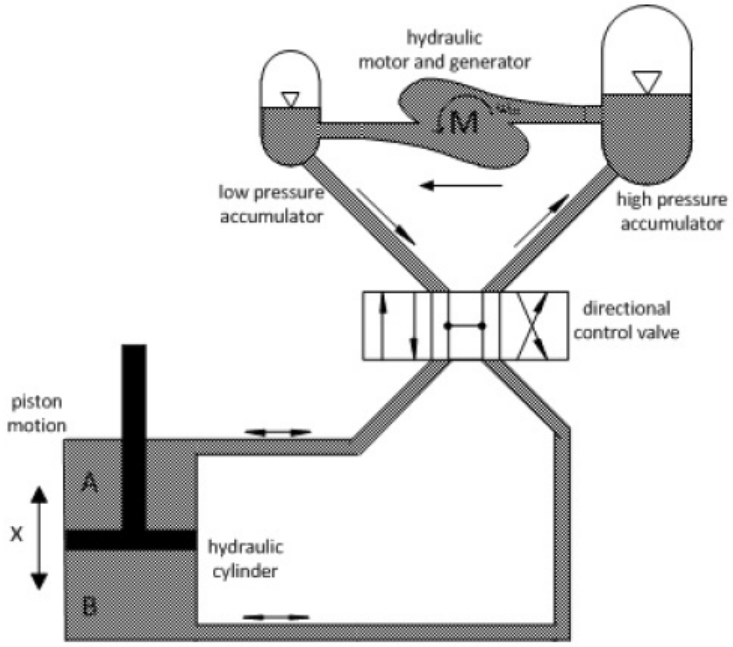

Figure 3.4: Hydraulic Power Take-Off System

The hydraulic PTO is a closed loop system, so assuming no leaks, the total mass in the system is a constant. If the hydraulic fluid is assumed to be incompressible, then from conservation of mass it is known that the volumetric flow of hydraulic fluid out of the piston must be equal to the volumetric flow into the HP accumulator, $\dot{V}_{piston} = \dot{V}_{HP_{in}}$. The volumetric flow from the piston is equal to the relative velocity times the cross-sectional area of the piston, $\dot{V}_{piston} = \dot{x}A_{pist}$. Applying conservation of mass inside the HP accumulator, an open system, the rate of change in volume of the hydraulic fluid in the HP accumulator must be equal to the volumetric flow in minus the volumetric flow out, as shown in Eq. (3.12). Similarly the rate of change in volume of the hydraulic fluid in the LP accumulator must be equal to the volumetric flow in minus the volumetric flow out, where the

volumetric flow out is equal to the volumetric flow into the piston, Eq. (3.13).

$$\frac{dV_{f,HP}}{dt} = \dot{V}_{HP,in} - \dot{V}_m \tag{3.12}$$

$$\frac{dV_{f,LP}}{dt} = \dot{V}_m - \dot{V}_{LP,out} \tag{3.13}$$

The accumulators are assumed to be initially filled and pressurized with nitrogen gas. Since the total volume of each of the accumulators is fixed, the rate of change of the volume of the hydraulic fluid must be equal and opposite to the rate of change of the volume of the nitrogen, as shown in Eq. (3.14). Assuming the nitrogen gas to be isentropic, the pressure in each accumulator as a function of time can be determined using the relationship defined in Eq. (3.15).

$$\frac{dV_{Ni}}{dt} = -\frac{dV_f}{dt} \tag{3.14}$$

$$P_{Ni}(0)V_{Ni}(0)^{1.4} = P_{Ni}(t)V_{Ni}(t)^{1.4} \tag{3.15}$$

Once the pressure difference across the accumulators is known, $\Delta p = p_{HP} - p_{LP}$, it can be used to calculate the force the PTO imparts on the WEC using Eq. (3.16). The power output of the hydraulic motor is highly dependent on the type of motor chosen and its control strategy. For the purpose of simplification, a hydraulic motor with a fixed rotational speed chosen to match a typical generator speed, $\omega_m = 1800$ rpm, and variable displacement as a function of the pressure difference and piston's volumetric flow was chosen, Eq. (3.17). The cross-sectional area above and below the piston is assumed to be equal, and frictional, inertial and pressure losses in the pipes and valves were neglected in this model.

$$F_{PTO} = -\Delta p A_{pist} sign(\dot{x}) \tag{3.16}$$

$$P_{out} = \tau\omega - m \quad where \quad \tau(\Delta p, \dot{V}_{pist}) \tag{3.17}$$

In addition to capturing the system dynamics described above, the hydraulic PTO system model must also account for other system constraints. The HP and LP accumulators are filled with hydraulic fluid and nitrogen gas that is initially pressurized. This pressurization imparts a force on the WEC that is equal to the initial pressure difference times the cross-sectional area of the piston. Two conditions must be met before the PTO system can produce power. First, the forces on the WEC must overcome the initial force of the PTO system in order to put the piston into motion. Second, the pressure difference across the HP and LP accumulators, $\Delta p = p_{HP} - p_{LP}$, must be great enough to put the hydraulic motor into motion.

3.4.2 PTO System Model

Now that an understanding of the hydraulic PTO system dynamics has been established, it is possible to develop a model. The PTO and Control subsystem that was defined in Figure 3.2, is shown in Figure 3.5. The relative motion between the plate and the buoy is the system input, and the power output by the hydraulic motor and the force the PTO system imparts on the WEC are the outputs. The volumetric flow from the piston is determined and then input into HP and LP Accumulator subsystems. The accumulator subsystems also take the volumetric flow across the motor as inputs and output the each accumulator's pressure. The

HP Accumulator subsystem that implements Eq. (3.12), (3.14) and Eq. (3.15) is shown in Figure 3.6. The LP Accumulator subsystem is very similar to Figure 3.6, except it implements Eq. (3.13), Eq. (3.14), and Eq. (3.15).

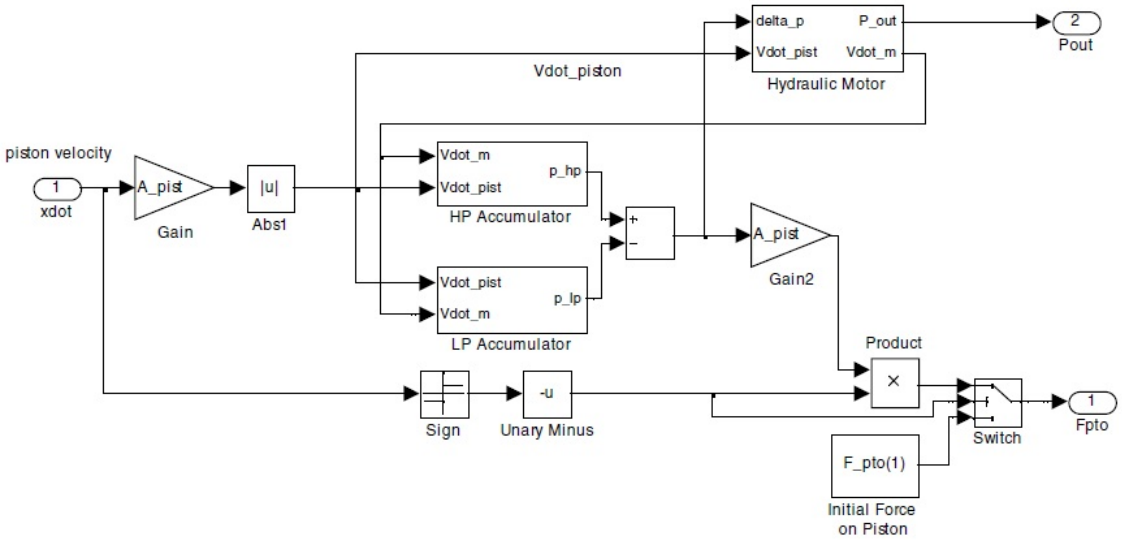

Figure 3.5: PTO and Control Subsystem for a Hydraulic PTO

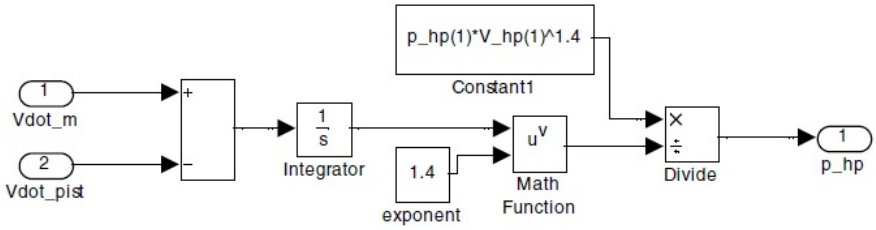

Figure 3.6: High Pressure Accumulator Subsystem

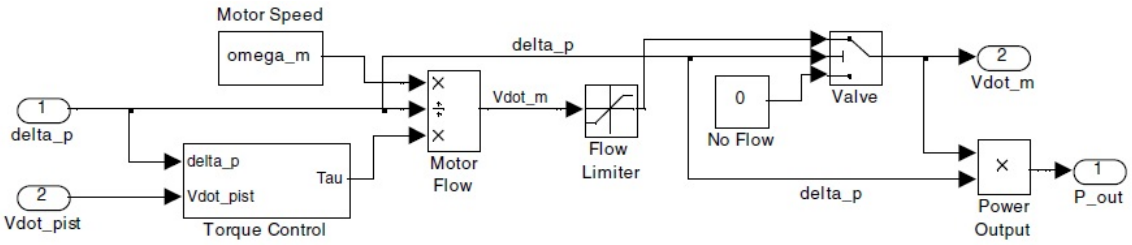

Figure 3.7: Hydraulic Variable Displacement Motor Subsystem

The Hydraulic Motor subsystem defined in Figure 3.5, is shown in Figure 3.7. This subsystem takes the pressure difference and piston's volumetric flow as inputs and outputs the volumetric flow through the motor and the motor's power output. For simplicity, the motor was modeled as a variable displacement, fixed rotational speed motor. The torque felt by the motor is determined by the Torque Control subsystem. The desired volumetric flow through the motors is determined by Eq. (3.18), but the actual volumetric flow allowed through the motor will be restricted by the Flow Limiter. In order for the motor to output power, the hydraulic motor needs to be put into motion. This condition is met by the Valve, which only opens once a finite pressure difference is met.

$$\dot{V}_m = \frac{\tau \omega_m}{\Delta p} \tag{3.18}$$

3.4.3 PTO System Results

The output of the hydraulic PTO system model for a given relative velocity with amplitude of 5m and frequency of 2 rad/s is shown in Figure 3.8. These results are for an initial pressure in the LP accumulator of 1.85 MPa, with an initial Nitrogen volume of 150 m^3, and initial pressure in the HP accumulator of 2.92 MPa, with

an initial Nitrogen volume of 400 m^3. The hydraulic cylinder has a diameter of 2.75 m, and the initial PTO force was set equal to 6,369 kN with a minimum motor flow rate 11 m^3/s and a maximum of 19 m^3/s. These dimensions and initial pressurizations are estimations of what a full scale two body point absorber would be designed for. The top plot in Figure 3.8 is the relative velocity, the middle plot shows the pressure difference across the accumulators and the solid line in the bottom plot is the instantaneous power available to the PTO, the points represent the power output by the hydraulic motor. It should be noted that the motor's power output is much more smoothed than the power available to the system. Also there is no power output until the initial required pressure difference is met, in this case equal to 1.5 times the initial pressure difference. Around the time of 1.5s there is no power output from the motor since the pressure difference drops below the threshold, thus ceasing the motor's motion.

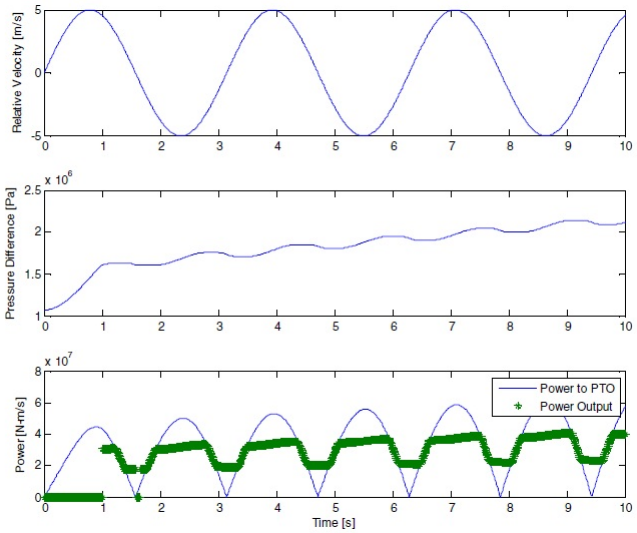

Figure 3.8: Sample Hydraulic PTO Model Output

3.5 Conclusions

This paper presents work towards creating generic models for WECs similar to existing generic turbine models in the wind industry. These models could be used to estimate power output at a potential installation site and would be beneficial to wave energy researchers, developers, investors and utilities alike. The focus of this paper is on developing time domain equations of motion for a two body heaving point absorber that consists of a buoy and a damping plate and using them to develop an overall modeling structure. Once systems and subsystems as well as their corresponding inputs and outputs are clearly defined, more detailed subsystems can be developed. The benefit of developing models this way is that the modularity easily allows for comparison of mooring configurations, device geometries, and PTO systems for a given wave climate. The second half of the paper discusses and defines the important characteristics and benefits of hydraulic PTOs when used for wave energy conversion. The WEC modeling structure defined in the first section is then used to develop a hydraulic PTO system model. Extensions of this work include further developing the two body point absorber model by subjecting the model to times series wave surface elevations representative of the Oregon wave climate. Another area of interest is to further develop the mooring subsystem to allow for more realistic mooring configurations. The hydraulic PTO system model could also be improved by accounting for the piston rod diameter and developing a more robust control mechanism. It would also be advantageous to develop a direct drive PTO system and compare a WECs response with a hydraulic PTO versus a direct drive PTO.

3.6 Acknowledgments

I would like to thank my co-authors, Dr. Brekken, Bret Bosma and Dr. Paasch for their insight and guidance developing my research and writing the paper. Thanks to Justin Hovland, Pukha-Lenee-Blum and Steve Meicke for stimulating conversations about wave energy and for paper editing. This work was completed through the Northwest National Marine Renewable Energy Center (NNMREC) which is supported by the Department of Energy under Award Number DE-FG36-08GO18179.

Chapter 4 – Combined Point Absorber and Hydraulic Power Take-Off System Model

The final result of the individual models presented in the previous manuscripts is a combined WEC Dynamics and Hydraulic PTO Model. Similar to the WEC dynamics modeling methodology presented in Figure 2.2, a methodology can be established for a WEC dynamics model that includes a PTO system model, as shown in Figure 4.1. This is done by taking the response solved for in the WEC Dynamics Model as an input to the Hydraulic PTO Model, and taking the PTO force as an input to the WEC Dynamics Model. The physical implementation of the Hydraulic PTO Model as a subsystem of the WEC Dynamics Model in MATLAB/Simulink is shown in Figure 3.2.

The combined WEC dynamics and PTO modeling methodology is used to model OSU's L10 two-body point absorber with a hydraulic PTO system. The hydraulic PTO system presented in Chapter 3 has been modified and resized for the L10, details of which are described in Appendix B. Using the combined WEC Dynamics and Hydraulic PTO Model, the L10's response when subject to wave surface elevation time-series from NDBC buoy 46229 in June 2008 (the same as used in Figure 2.19 for the L10 model without a PTO system) is shown in Figure 4.2. The L10's displacement when subject to the incoming wave is shown on the top, and the relative velocity between the buoy and spar/plate is shown in the middle. This relative velocity is used as input to the Hydraulic PTO subsystem which determines the hydraulic piston's volumetric flow, and the flow across the hydraulic motor, both of which are shown on the bottom of Figure 4.2. In Fig-

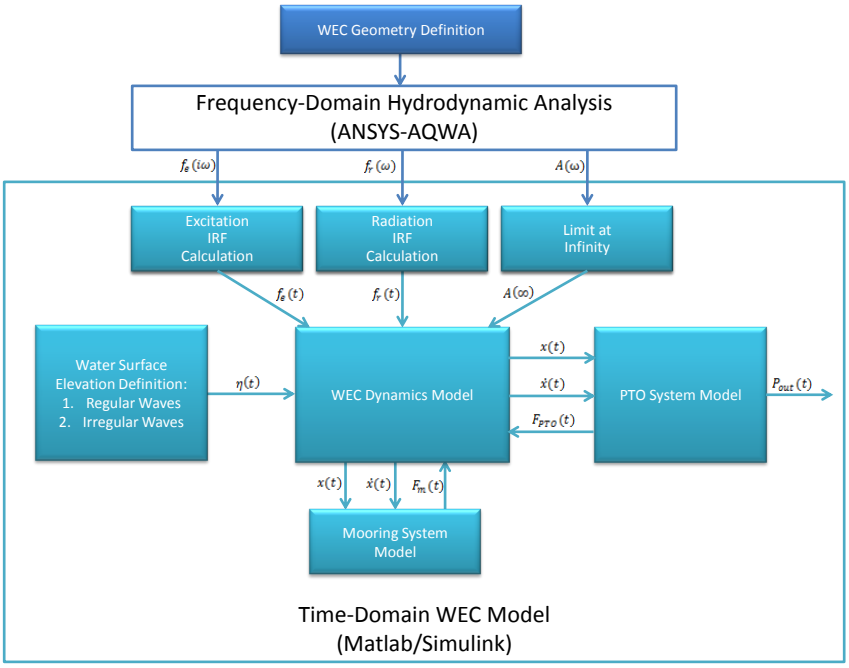

Figure 4.1: Flowchart of Combined WEC and PTO Modeling Methodology

ure 4.3 the pressure difference across the HP and LP accumulators is shown on the top. The HP and LP accumulators act as temporary energy storage, and allow for the motor's smoothed power output by comparison to the instantaneous power available to the PTO. The instantaneous power and the smoothed hydraulic motor power output are shown on the bottom of Figure 4.2. Results from the combined WEC Dynamics and Hydraulic PTO Model attest to the advantage of implementing a hydraulic PTO system over a direct drive PTO system because the hydraulic systems provides power smoothing, even when subject to stochastic ocean waves.

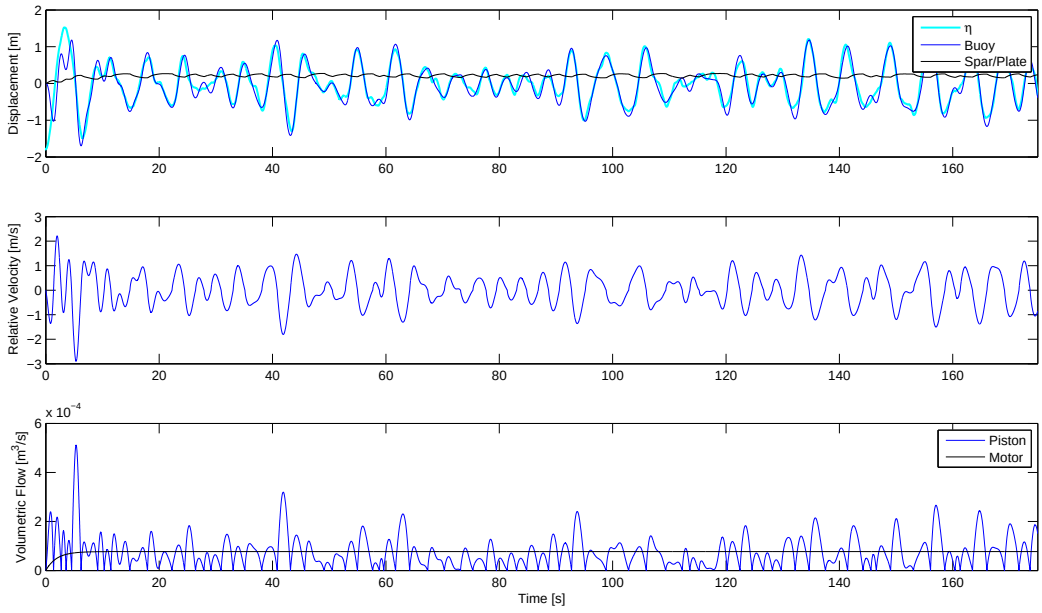

Figure 4.2: L10 Irregular Wave Response: (top) Wave and WEC Displacement, (middle) Relative Velocity, (bottom) Volumetric Flow

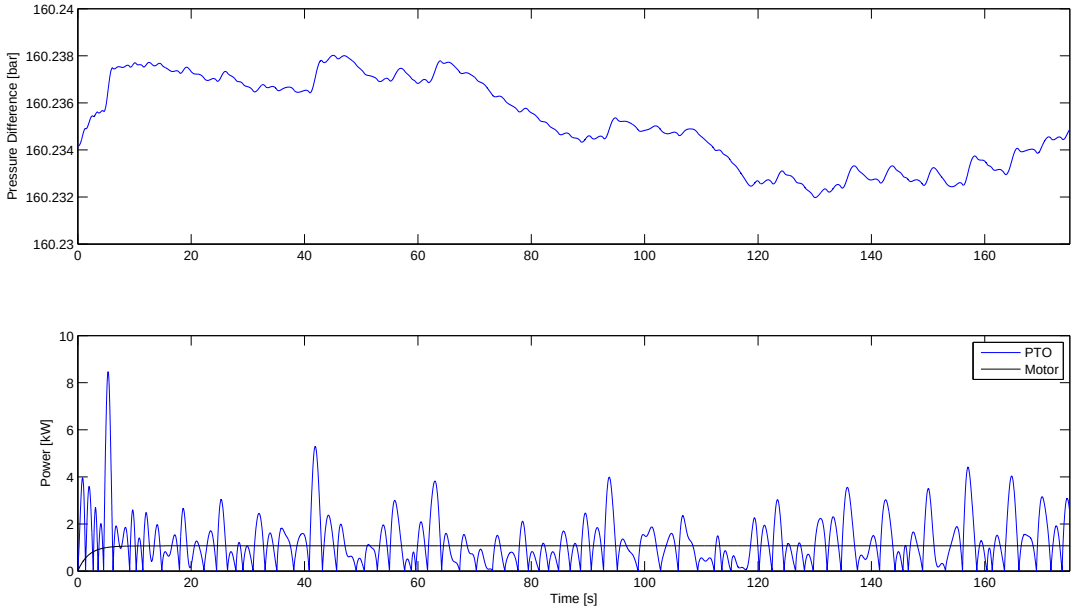

Figure 4.3: L10 Hydraulic PTO: (top) Pressure Difference, (bottom) Power

Chapter 5 – Conclusions

In order to promote development of the wave energy industry, researchers, developers, and utilities need to estimate a WEC's performance when subject to a potential site's wave climate. The manuscripts presented in this thesis describe two independent models implemented in MATLAB/Simulink that were developed to bridge this gap. In the first manuscript the development of a point absorber WEC Dynamics Model was described. The WEC Dynamics Model takes the incoming wave as its input, and solves for the point absorber's response. The model was first validated by comparison to experimental data for a single-body point absorber with complex geometry. Then, the WEC dynamics modeling methodology was applied to model OSU's L10 two-body point absorber. The second manuscript describes development of a Hydraulic PTO Model. The Hydraulic PTO Model takes the point absorber's relative velocity as its input, and solves for the power output of the hydraulic motor. Finally, in Chapter 4 results from the combined WEC Dynamics and Hydraulic PTO Model were presented when used to model OSU's L10 two-body point absorber with a hydraulic PTO system.

Future extensions of the WEC Dynamics Model include extending the single-body point absorber dynamics model to include all 6 degrees of freedom, and validating the two-body point absorber dynamics model by comparison to experimental wave tank data. Also, the combined WEC Dynamics and Hydraulic PTO Model will be used to develop optimal control strategies.

Bibliography

[1] Aquamarine Power - Producing clean sustainable electricity from wave energy. http://www.aquamarinepower.com/.

[2] Columbia Power Technologies. http://www.columbiapwr.com/.

[3] National Data Buoy Center. http://www.ndbc.noaa.gov/.

[4] Neptune Wave Power. http://www.neptunewavepower.com/.

[5] Ocean Power Technologies. http://www.oceanpowertechnologies.com/.

[6] Pelamis Wave Power. http://www.pelamiswave.com/.

[7] Wave Dragon. http://www.wavedragon.net/.

[8] Wave Energy Wave Power Clean Renewable Electricity Generation - Wavegen. http://www.wavegen.co.uk/.

[9] Wavebob. http://www.wavebob.com/.

[10] ANSYS Inc. ANSYS AQWA 13.0. 275 Technology Drive, Canonsburg, PA.

[11] L. Armbruster, D. Arnold, B. Cable, and B. Hockenmaier. Survery and Assessment of Renewable Ocean Energy Technologies. Technical Report TR-2325-OCN, NAVFAC ESC, Port Hueneme, California 93043-4370, December 2009.

[12] A. Babarit, M. Guglielmi, and A.H. Clement. Declutching control of a wave energy converter. *Ocean Engineering*, 36:1015–1024, Sept 2009.

[13] J. Cândido and P. Justino. Modelling, control and pontryagin maximum principle for a two-body wave energy device. *Renewable Energy*, 36(5):1545–1557, May 2011.

[14] B. Child and V. Venugopal. Interaction of waves with an array of floating wave energy devices. In *Proceedings of the 7th European Wave and Tidal Energy Conference*, Porto, Portugal, 2007.

[15] W.E. Cummins. The impulse response function and ship motions. *Schiffstechnik*, 9:101–109, 1962.

[16] R. Dean and R. Dalrymple. *Water wave mechanics for engineers and scientists*. World Scientific, 1991.

[17] Department of the Navy. Environmental Assessment for Proposed Wave Energy Technology Project. Technical report, Naval Facilities Engineering Command Pearl Harbor, Hawaii 96860-3134, Marine Corps Base Hawaii, Kaneohe Bay, Hawaii, January 2003.

[18] H. Eidsmoen. Simulation of a slack-moored heaving-buoy wave-energy converter with phase control. Technical report, Division of Physics, Norwegian University of Science and Technology, Trondheim, Norway, 1996.

[19] H. Eidsmoen. Tight-moored amplitude-limited heaving-buoy wave-energy converter with phase control. *Applied Ocean Research*, 20(3):157–161, June 1998.

[20] D. Elwood, A. Schacher, K. Rhinefrank, J. Prudell, S. Yim, E. Amon, T.K.A. Brekken, and A. von Jouanne. Numerical modeling and ocean testing of a Direct-Drive wave energy device utilizing a permanent magnet linear generator for power Take-Off. *ASME Conference Proceedings*, 2009(43444):817–824, January 2009.

[21] A. F. Falcão. Modelling and control of oscillating-body wave energy converters with hydraulic power take-off and gas accumulator. *Ocean Engineering*, 34(14-15):2021–2032, October 2007.

[22] A. F. Falcão. Phase control through load control of oscillating-body wave energy converters with hydraulic PTO system. *Ocean Engineering*, 35(3-4):358–366, March 2008.

[23] J. Falnes. On non-causal impulse response functions related to propagating water waves. *Applied Ocean Research*, 17(6):379–389, December 1995.

[24] J. Falnes. *Ocean waves and oscillating systems: linear interactions including wave-energy extraction*. Cambridge University Press, 2002.

[25] J. Falnes and P. Lillebekken. Budal's latching controlled-buoy type wave-power plant. In *5th European Wave Energy Conference*, 2003.

[26] R. Henderson. Design, simulation, and testing of a novel hydraulic power take-off system for the Pelamis wave energy converter. *Renewable Energy*, 31:271–283, Feb 2006.

[27] E.R. Jefferys. *Power from Sea Waves*, Device Characterisation Device Characterisation, pages 413–437. Academic Press, 1980.

[28] C. Josset, A. Babarit, and A.H. Clement. A wave-to-wire model of the SEAREV wave energy converter. *Proceedings of the Institution of Mechanical Engineers, Part M: Journal of Engineering for the Maritime Environment*, 221:81–93, 2007.

[29] F. Kara. Time domain prediction of power absorption from ocean waves with latching control. *Renewable Energy*, 35(2):423–434, February 2010.

[30] M.T. Koopmans, S. Meicke, I.Y. Tumer, and R. Paasch. Experimental polymer bearing health estimation and test stand benchmarking for wave energy converters (submitted). In *Annual Conference of the Prognostics and Health Management Society*, 2011.

[31] P. Lenee-Bluhm, R. Paasch, and H. T. Özkan-Haller. Characterizing the wave energy resource of the US pacific northwest. *Renewable Energy*, 36(8):2106–2119, August 2011.

[32] Y. Li, Y-H. Yu, M. Previsic, E. Nelson, and R. Thresher. Numerical and experimental investigation of a floating point absorber wave energy converter under extreme wave condition.

[33] The MathWorks Inc. MATLAB 7.9.0, SIMULINK 7.4. 3 Apple Hill Drive, Natick, Massachussets.

[34] M. McCormick. *Ocean Wave Energy Conversion*. Dover Publications, 2007.

[35] P. Ricci, J. B. Saulnier, A. F. Falcão, and M. T. Pontes. Time-Domain models and wave energy converters performance assessment. In *Proceedings of the ASME 27th International Conference on Offshore Mechanics and Arctic Engineering*, Estoril, Portugal, June 2008.

[36] K. Ruehl, T.K.A. Brekken, B. Bosma, and R. Paasch. Large-scale ocean wave energy plant modeling. In *2010 IEEE Conference on Innovative Technologies for an Efficient and Reliable Electricity Supply (CITRES)*, pages 379–386, Waltham, MA, September 2010.

[37] J. Shek, D. Macpherson, M. Mueller, and J. Xiang. Reaction force control of a linear electrical generator for direct drive wave energy conversion. *Renewable Power Generation, IET*, 1:17–24, 2007.

[38] A.L. Silver, M.J. Hughes, R.E. Conrad, S.S. Lee, J.T. Klamo, and J.T. Park. Evaluation of Multi-Vessel ship motion prediction codes. Technical Report NSWCCD-50-TR–2008/070, Naval Surface Warfare Center Carderock Division 9500 Macarthur Boulevard West Bethesda, MD, September 2008.

[39] M.J. Tucker, P.G. Challenor, and D.J.T. Carter. Numerical simulation of a random sea: a common error and its effect upon wave group statistics. *Applied Ocean Research*, 6(2):118–122, April 1984.

[40] H. Yavuz, A. McCabe, G. Aggidis, and M. Widden. Calculation of the performance of resonant wave energy converters in real seas. *Proceedings of the Institution of Mechanical Engineers, Part M: Journal of Engineering for the Maritime Environment,*, 220:117–128, Jan 2006.

[41] H. Yavuz, T J Stallard, A P McCabe, and G A Aggidis. Time series analysis-based adaptive tuning techniques for a heaving wave energy converter in irregular seas. *Proceedings of the Institution of Mechanical Engineers*, 2006.

[42] Y-H. Yu and Y. Li. Preliminary results of a RANS simulation for a floating point absorber wave energy system in extreme wave conditions. In *Proceedings of the ASME 30th International Conference on Ocean, Offshore and Arctic Engineering*, Rotterdam, The Netherlands, June 2011.

APPENDICES

Appendix A – Mooring Force Determination

The mooring system defined in the WEC Dynamics Model is based on the experimental mooring configuration used by Li [32]. The side and top views of this mooring configuration are shown in Figure A.1 and Figure A.2 respectively. The mooring system consists of 8 lines in total, each with stiffness, $k_m = 160\ [kN/m]$ and initial length $l_m = 1.7\ [m]$.

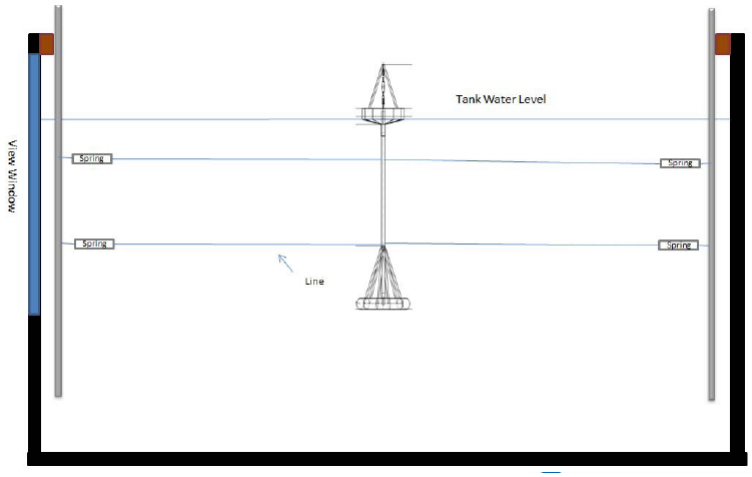

Figure A.1: Experimental Mooring Configuration: Side View, courtesy of RE Vision

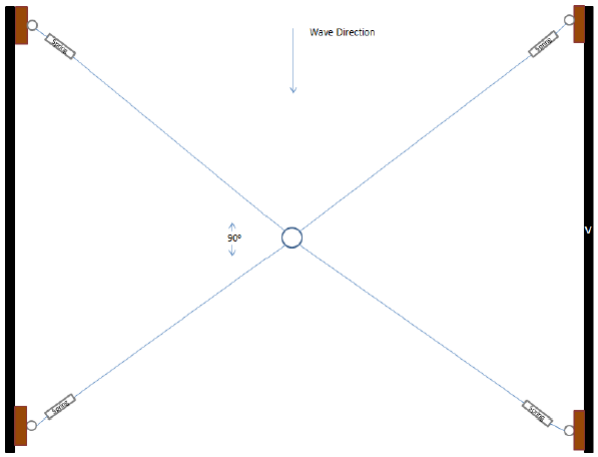

Figure A.2: Experimental Mooring Configuration: Side View, courtesy of RE Vision

Since the WEC Dynamics Model assumes heave motion only, when the point absorber heaves in the x direction, the mooring line will stretch from its initial length to a length of l'_m according to the trigonometric relationship defined in Figure A.3. Accordingly, the total force in each mooring line is defined in Eq. A.1.

$$F_m = k_m(l'_m - l_m) \tag{A.1}$$

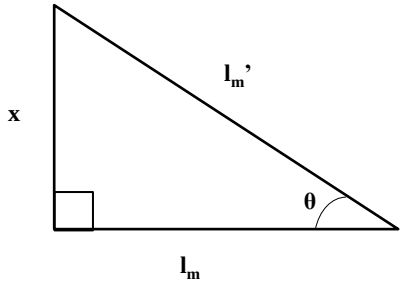

Figure A.3: Mooring System Heave Displacement

From the total force in each mooring line, the force felt by the WEC in the heave direction can be determined as a function of the heave displacement and the initial mooring line length using trigonometry according to Eq. A.2. Since there are 8 mooring lines, the total heave force felt by the WEC is defined by Eq. A.3.

$$\begin{aligned} F_{m,x} &= k_m(l'_m - l_m)sin(\theta) \\ &= k_m(l'_m - l_m)x/l'_m \\ &= k_m x(1 - l_m/l'_m) \\ &= k_m x\left(1 - \frac{l_m}{\sqrt{{l_m}^2 + x^2}}\right) \end{aligned} \tag{A.2}$$

$$F_{m,x,tot} = 8k_m x\left(1 - \frac{l_m}{\sqrt{{l_m}^2 + x^2}}\right) \tag{A.3}$$

Appendix B – L10 Hydraulic PTO Model

The hydraulic PTO system model in the combined WEC Dynamics and Hydraulic PTO Model for the L10 two-body point absorber has the same configuration as the Hydraulic PTO Model, shown in Figure 3.4. However, some changes were made in the combined model to better suit the size of the L10. Additionally, the piston's rod diameter was accounted for, and instead of modeling a variable displacement hydraulic motor (as was modeled in the second manuscript), the L10's hydraulic PTO system is modeled with a fixed displacement motor.

The hydraulic piston modeled in the combined WEC Dynamics and Hydraulic PTO Model is shown in Figure B.1. This is different from Eq. 3.16 which doesn't account for the difference between the area on the top of the piston, $A_{top} = \pi D_{bore}^2/4$, and the area on the bottom of the piston, $A_{bot} = \pi(D_{bore}^2 - D_{rod}^2)/4$, due to the presence of the rod.

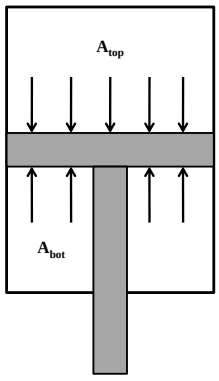

Figure B.1: Hydraulic Piston

For the L10's modeled hydraulic PTO system, the hydraulic piston's measurements are: $D_{bore} = 0.0152\ m$ and $D_{rod} = 0.0102\ m$. The hydraulic system is initially pressurized with $p_{HP} = 1.6125\ e07\ Pa$ in the HP accumulator, and at $p_{LP} = 101325\ Pa$ (atmospheric pressure) in the LP accumulator. Initially, the hydraulic piston has the p_{HP} on the bottom, and p_{LP} on the top. When the hydraulic piston moves, the HP and LP sides will change according to the direction the piston is moving. As a result, the force felt on the PTO system will also change according to the piston's direction of motion, as defined in Eq. B.1, and the instantaneous power available to the PTO system is defined by Eq. B.2.

$$\begin{aligned} if\ \dot{x} >= 0, \quad & F_{PTO} = p_{HP}A_{bot} - p_{LP}A_{top} \\ if\ \dot{x} < 0, \quad & F_{PTO} = p_{LP}A_{bot} - p_{HP}A_{top} \end{aligned} \tag{B.1}$$

$$P_{PTO} = F_{PTO}\dot{x} \tag{B.2}$$

Since the hydraulic system is initially pressurized, buoyancy forces must be defined for the buoy and spar/plate so that Eq. 3.5 and Eq. 3.6 initially sum to zero. In order to achieve a zero force summation, the buoyancy forces are set equal to the initial PTO force, as defined in Eq. B.3.

$$F_{b_1} = F_{b_2} = F_{pto,i} = 1615.6\ N \tag{B.3}$$

Additionally, the hydraulic motor in the combined WEC Dynamics and Hydraulic PTO Model is modeled as a fixed displacement motor, unlike the Hydraulic PTO Model governed by Eq. 3.17 and Eq. 3.18. The fixed displacement motor modeled has a fixed volumetric displacement per revolution, $V_g = 0.00002\ m^3$, and

calculates the motor's volumetric flow, $\dot{V}_m$ according to Eq. B.4.

$$\dot{V}_m = \frac{V_g \omega_m}{2\pi} \tag{B.4}$$

For a fixed displacement motor the torque felt on the motor due to the pressure difference across the accumulators is governed by Eq. B.5, and the power out of the hydraulic motor is defined by Eq. B.6

$$\tau_m = \frac{V_g \Delta p}{2\pi} \tag{B.5}$$

$$P_{out} = \dot{V}_m \Delta p \tag{B.6}$$